Reappraisal of the Magma-rich versus Magma-poor Rifted Margin Archetypes

Julie Tugend[1*], Morgane Gillard[1], Gianreto Manatschal[1], Michael Nirrengarten[2], Caroline Harkin[3], Marie-Eva Epin[1], Daniel Sauter[1], Julia Autin[1], Nick Kusznir[3] & Ken McDermott[4]

[1]*Institut de Physique du Globe de Strasbourg; CNRS-UMR 7516, Université de Strasbourg, 1 rue Blessig, F-67084 Strasbourg Cedex, France.*
[2]*Département Géosciences et Environnement, Université de Cergy-Pontoise, Neuville-sur-Oise, France.*
[3]*Department of Earth, Ocean & Ecological Sciences, University of Liverpool, Liverpool L69 3GP, United Kingdom*
[4]*ION, 31 Windsor St., Chertsey, KT16 8AT, United Kingdom*

[*]Correspondence (julie.tugend@sorbonne-universite.fr) Current address: *Sorbonne Université, CNRS-INSU, Institut des Sciences de la Terre Paris, ISTeP UMR 7193, F-75005 Paris, France*)

Words of text: 9887
References: 140
Figures: 8

Running title: Reappraisal of Magma-poor/magma-rich archetypes

Abstract (200/200)

Rifted margins are commonly defined as magma-poor or magma-rich archetypes based on their morphology. We re-examine the prevailing model inferred from this classification that magma-rich margins have excess decompression melting at lithospheric breakup compared with steady state seafloor spreading, while magma-poor margins have inhibited melting. We investigate the magmatic budget related to lithospheric breakup along two high-resolution long-offset deep reflection seismic profiles across the SE-Indian (magma-poor) and Uruguayan (magma-rich) rifted margins.

Resolving the magmatic budget is difficult and several interpretations can explain our seismic observations, implying different mechanisms to achieve lithospheric breakup and melt production for each archetype. We show that the Uruguayan and other magma-rich margins may indeed involve excess decompression melting compared with steady-state seafloor

spreading but could also be explained by a gradual increase with an early onset relative to crustal breakup. A late onset of decompression melting relative to crustal breakup enables mantle exhumation characteristic of magma-poor margin archetypes (e.g. SE-India).

Despite different volumes of magmatism, the mechanisms suggested at lithospheric breakup are comparable between both archetypes. Considerations on the timing of decompression melting onset relative to crustal thinning may be more important than the magmatic budget to understand the evolution and variability of rifted margins.

Rifted margins used to be classified as 'volcanic' or 'non-volcanic' (e.g. Mutter *et al.* 1988; White & McKenzie 1989; Boillot & Coulon 1998). Used in the strictest sense, this classification quickly became somewhat binary and confusing (Mutter 1993), implying different mechanisms for lithospheric thinning and breakup. Because magmatism is observed even in settings initially considered as non-volcanic (e.g. Whitmarsh *et al.* 2001a/b; Desmurs *et al.* 2001), this terminology has been later adjusted to 'magma-poor' ('magma-starved') or 'magma-rich' ('magma-dominated') rifted margins (e.g. Sawyer *et al.* 2007; Reston 2009; Reston & Manatschal 2011; Doré & Lundin 2015). The definition of these end-member archetypes relies on the identification of a number of morphological features considered as characteristic for magma-poor or magma-rich rifted margins (e.g. Menzies *et al.* 2002; Reston 2009; Franke 2013; Doré and Lundin 2015). This terminology leads to assumptions on the magmatic budget: magma-rich rifted margins have a high magmatic budget during rifting and at lithospheric breakup while magma-poor margins have a very low magmatic budget. In particular, magma-rich margins are thought to have excess decompression melting, often associated with elevated asthenosphere temperatures, compared with steady-state sea-floor spreading. In contrast, magma poor margins are suggested to have inhibited decompression melting. However, this simplification based on the magmatic budget can be misleading. In this work, we re-examine this prevailing model. In fact, most rifted margins show complex and polyphase tectono-magmatic evolutions during rifting and at lithospheric breakup, preceding steady-state seafloor spreading onset and can preserve characteristic features of both end-member archetypes. Magma-poor rifting can precede magma-rich lithospheric breakup (e.g. North-West shelf of Australia, Belgarde *et al.* 2015; Mid-Norwegian margin, e.g. Lundin & Doré 2011; Gernigon *et al.* 2015) and vice versa (e.g. India-Seychelles, Armitage *et al.* 2012). Deciphering the interaction between tectonic and magmatic processes at rifted margins is, therefore, important to understand the mechanisms controlling their rift-to-drift transition whether they are considered as magma-poor or magma-rich.

Magmatic processes occurring at the rift-to-drift transition, ie. related to lithospheric breakup, are recorded continentward of the first unambiguous oceanic domains, in so-called 'transitional' (Welford *et al.* 2010; Sibuet & Tucholke 2013), 'embryonic' (Jagoutz *et al.* 2007), 'proto-oceanic' (Gillard *et al.* 2015) or 'outer domains' (Péron-Pinvidic *et al.* 2013; Peron-Pinvidic & Osmundsen 2016). At the rift-to-drift transition, melt production appears transient (Gladczenko *et al.* 1997; Nielsen & Hopper 2004; Perez-Guissinyé *et al.* 2006) and tectonic deformation is not yet localized at a stable spreading centre (Gillard *et al.* 2015, 2016b). This domain replaces the classical Continent-Ocean-Boundary (COB) (Peron-Pinvidic &

Osmundsen 2016), difficult to identify unambiguously (e.g. Eagles *et al.* 2015). The nature of the basement remains poorly constrained and the underlying lithosphere is often described as transitional or hybrid between continental and oceanic (Welford *et al.* 2010; Sibuet & Tucholke 2013; Franke 2013; Gillard *et al.* 2015, 2017; Peron-Pinvidic & Osmundsen 2016).

We describe and discuss observations from two high-resolution long-offset deep reflection seismic profiles provided by ION Geophysical across the South-East (SE) Indian and Uruguayan rifted margins. These examples are respectively considered as representative of magma-poor (e.g. Nemčok *et al.* 2013; Sinha *et al.* 2016; Haupert *et al.* 2016) and magma-rich rifted margins (e.g. Gladczenko *et al.* 1997; Blaich *et al.* 2011; Franke 2013). We apply the same seismic interpretation approach to describe and characterize their first-order architecture and magmatic budget. We focus on the location, timing and amount of magmatic additions emplaced at lithospheric breakup within ultra-distal rifted margins, in so-called proto-oceanic domains. The determination of the magmatic budget and the nature of the basement remains non-unique based on seismic reflection or from other indirect geophysical methods. For that reason, we present several hypotheses that can fit our observations for both examples. These alternative interpretations represent end-member scenarios for the magmatic budget at lithospheric breakup resulting in different architectures of proto-oceanic domains. Based on these three ‘end-member’ interpretations, we suggest distinct mechanisms to achieve lithospheric breakup implying variable melt production, applicable to both rifted margin archetypes (magma-poor or magma-rich).

More generally, our work highlights the difficulty in determining a magmatic budget at rifted margins, showing the limitations and strong assumptions inherent to classifications based on this criterion. Despite different volumes of magmatism, the different mechanisms suggested at lithospheric breakup appear comparable between the magma-poor and magma-rich archetypes. Considerations on the onset of decompression melting relative to crustal thinning appear equally, if not more important, than the overall magmatic budget to understand the evolution and worldwide variability of rifted margins.

Dataset and interpretational approach

Reflection seismic data

We describe and interpret two industrial high-resolution long-offset deep reflection seismic profiles acquired, processed and provided by ION Geophysical. Located across the SE-Indian and Uruguayan rifted margins, these two profiles are part of the IndiaSPAN and

UruguaySPAN projects (locations Fig. 1a and 2a). These surveys are respectively composed of approximately 27,700 km and 2,800 km of seismic data acquired using powerful deep-penetrating sources. Some details on acquisition parameters of these two seismic surveys are available from ION Geophysical website (*http://www.iongeo.com/Data_Library/India/* and *http://www.iongeo.com/Data_Library/South_America/Uruguay/)* and described in Nemčok *et al.* (2013) for the IndiaSPAN project. Kirchhoff prestack time and depth migrations (PSTM and PSDM) were performed on both seismic surveys following proprietary ION Geophysical processing workflow (example of processing workflow in Sauter *et al.* 2016). PSTM profiles were initially available with a 18s record length. PSDM profiles image the crustal architecture down to 25 km for the IndiaSPAN and to 40 km for the UruguaySPAN.

Our interpretational work remained focused along the two seismic profiles (locations Fig. 1b and 2b). Previous observations and interpretations are nevertheless available for the SE-Indian margin, some also focused on the same seismic profile (e.g. Radhakrishna *et al.* 2012; Nemčok *et al.* 2013; Mangipudi *et al.* 2014; Pindell *et al.* 2014; Haupert *et al.* 2016). Seismic data and interpretations are available from other surveys offshore Uruguay or from adjacent lines also part of the UruguaySPAN (e.g. Franke *et al.* 2007; Soto *et al.* 2011; Clerc *et al.* 2015).

[Figure 1 about here: Portrait, 2 columns: 135 x 204 mm]

[Figure 2 about here: Portrait, 2 columns: 135 x 204 mm]

Methodology

We applied on both case examples a seismic interpretation approach similar to the one described in Tugend *et al.* (2015) and summarized hereafter. We adapted the workflow to the interpretation of first order characteristic features of both magma-poor and magma-rich rifted margins. First, we focused on the definition of first-order interfaces (where observable) on both PSTM and PSDM seismic lines, including the seafloor, top basement (i.e. base syn-tectonic sediments or base passive infill), base of Seaward Dipping Reflectors (SDRs)/extrusive and seismic Moho. Second, based on descriptions of the stratigraphic architecture and its relation to the underlying basement, we identified potential low- and high-β extensional settings (Wilson *et al.* 2001), this later being associated to tectonically exhumed surfaces (Wilson *et al.* 2001; Tugend *et al.* 2015). Third, we identified and characterized different forms of magmatic additions (e.g. SDRs, sill intrusions, volcanic edifices; Planke *et al.*, 2000; 2005; Calvès *et al.* 2011). The relation of these magmatic additions to key stratigraphic horizons (pre-, syn-, post-rift), where observable, can provide information on the timing of magma-emplacement relative to the evolution of the margin.

The identification of first-order interfaces on PSDM sections illustrates the evolution of total accommodation space (between sea level and top of acoustic basement; i.e. the present-day depth to top basement) and crustal thickness (between top of acoustic basement and seismic Moho). In the case of magma-rich rifted margins, defining the interface between the base of SDRs/extrusive magmas is often difficult. Determining the accommodation space created during rifting remains thus challenging, as well as the relative proportion between magmatic additions and sediments.

Terminology

Based on this workflow, we define a set of first-order comparable architectural features that we consider as building blocks, ie. corresponding to structural domains of rifted margins. From continent to ocean, we distinguish the proximal, necking, hyperthinned, exhumed mantle, proto-oceanic and oceanic domains based on the terminology and definitions of Peron-Pinvidic *et al.* 2013; Sutra *et al.* 2013; Tugend *et al.* 2015; Peron-Pinvidic *et al.* 2017; Gillard *et al.* 2015. For the purpose of this contribution, we do not discriminate between the necking and hyperthinned domain and refer to the combination of both as 'thinned domain'. These structural domains are considered to correspond to genetic domains recording the interplay between successive extensional and/or magmatic processes (e.g. Lavier & Manatschal 2006; Péron-Pinvidic & Manatschal 2009; Sutra *et al.* 2013). Related processes are, however, also likely to interact and overlap in time and space during rifted margin evolution (e.g. Péron-Pinvidic & Manatschal 2009). As a result, structural domains are often not delimited by strict boundaries and the passage from one to the other is likely more complex and in some examples gradual (Peron-Pinvidic *et al.* 2013).

In this work, we distinguish 'crustal' and 'lithospheric' breakup. We consider that crustal breakup is achieved when the continental crust of two conjugate rifted margins is separated. Following Minshull *et al.* 2001, crustal breakup (referred to as 'continental breakup' in Minshull *et al.* 2001) corresponds to the seaward limit of stretched continental crust. We define lithospheric breakup as a tectono-magmatic process recording the rift-to-drift transition (Péron-Pinvidic & Osmundsen 2016) at proto-oceanic domains (Gillard *et al.* 2015) defined continentward of the first unambiguous oceanic domain. Following Gillard *et al.*, 2015; 2016b, we consider that lithospheric breakup is achieved through the emplacement of a steady-state, self-sustaining, seafloor-spreading system, i.e. corresponding to stable and localized oceanic accretion. As emphasized by Minshull *et al.* 2001 and further discussed in this work, the location and timing of 'crustal breakup' may or may not correspond to 'lithospheric breakup'.

The SE-India rifted margin case example

Geological setting and first-order tectono-magmatic context

The SE-Indian rifted margin was once conjugate to East Antarctica through the Enderby Basin, Princess Elizabeth Trough and Davis Sea Basin (e.g. Powell *et al.* 1988; Ramana *et al.* 1994; Reeves & de Wit 2000; Lal *et al.* 2009; Radhakrishna *et al.* 2012; Sinha *et al.* 2016). The present-day structure of the SE-Indian rifted margin results from a complex and polyphase breakup history involving India, Antarctica and Australia (e.g. Powell *et al.* 1988; Gaina *et al.* 2003; Subrahmanyam & Chand 2006; Lal *et al.* 2009). Between India and Antarctica, the occurrence of a complex breakup, related to the formation of the Elan Bank microcontinent, now preserved offshore Antarctica, is generally accepted (Gaina *et al.* 2003, 2007; Radhakrishna *et al.* 2012; Sinha *et al.* 2016; Talwani *et al.* 2016). Still, due to uncertainties on the identification of magnetic anomalies, the exact fit of Elan Bank as well as the detailed timing of rifting and lithospheric breakup remains debated. Elan Bank is either interpreted as conjugate to the Krishna-Godavari (Radhakrishna *et al.* 2012; Sinha *et al.* 2016) or to the Mahanadi segment (Talwani *et al.* 2016) of the SE-Indian margin (Fig. 1). Rifting seems to have started already during late Early Jurassic time (Nemčok *et al.* 2013; Sinha *et al.* 2016 and references therein), but the main rift event shaping the SE-Indian margin likely occurred at the beginning of Early Cretaceous time (Powell *et al.* 1988; Lal *et al.* 2009; Sinha *et al.* 2016 and references therein). Rifting might not be synchronous along the entire margin (e.g. Sinha *et al.* 2016) that appears quite segmented. From southwest to northeast (Fig. 1), the Cauvery, Palar-Penmar, Krishna-Godavari, Mahanadi and Bengal basins are characterized by variable transtensional deformation and magmatic budget (e.g., Subrahmanyam & Chand 2006; Radhakrishna *et al.* 2012; Nemčok *et al.* 2013; Talwani *et al.* 2016 and references therein).

In the Bay of Bengal, two oceanic ridges are identified trending roughly N-S: the 85°E ridge terminating toward the Mahanadi segment (e.g. Curray & Munasinghe 1991; Choudhuri *et al.* 2014) and the Ninetyeast ridge (e.g. Coffin *et al.* 2002) further east (Fig. 1). The Ninetyeast ridge is commonly interpreted to mark the Kerguelen hotspot track. There is no general agreement on the nature of the 85°E ridge. It is interpreted either as a fracture zone (Talwani *et al.* 2016 and references therein), as a hotspot track, or a hotspot track along a transform (Curray & Munasinghe 1991; Choudhuri *et al.* 2014), the associated plume being debated. The Rajmahal Traps (~118 Ma, (Coffin *et al.* 2002; Kent *et al.* 2002) cropping out onshore East India, are interpreted as the Early Cretaceous magmatic record of the Kerguelen plume (e.g. Coffin *et al.* 2002; Kent *et al.* 2002; Baksi *et al.* 1987; Olierook *et al.* 2016) either associated to the Ninetyeast and/or 85°E ridge.

We focus on a high-resolution reflection seismic profile provided by ION Geophysical, striking NW-SE across the Krishna-Godavari segment of the SE-India rifted margin (Fig. 1). This area presents the characteristic features generally attributed to magma-poor hyperextended rifted margins, including extremely thinned continental crust and exhumed mantle (Nemčok *et al.* 2013; Radhakrishna *et al.* 2012; Sinha *et al.* 2016; Pindell *et al.* 2014; Haupert *et al.* 2016). The 85^{o}E and 90^{o}E ridges identified in the Bay of Bengal probably correspond to hotspot-transform tracks (Fig. 1) but they were formed only after rifting and lithospheric breakup occurred along the segment considered in this work as suggested by Gaina *et al.* (2007); Sinha *et al.* (2016).

Seismic observations

Definition of first order interfaces

Seafloor delimits the present-day shelf break at about distance 15 km and deepens oceanward, reaching ~3 km depth in the Bay of Bengal (Fig. 3). *Top basement*, where characterized by high amplitude reflectors, is fairly well recognizable along the profile (Fig. 3). Continentward, from 0 to ~80 km, top basement progressively deepens from ~2 to 9 km depth and is characterized by sharp topographic variations. It corresponds to the interface between the base of syn-rift sediments and acoustic basement (possibly also including pre-rift sediments or corresponding to crystalline basement). From ~80 to ~150 km, we define top basement as the base of passive infill (as indicated by onlap/downlap geometry of overlaying sediments, Fig. 3c). Underneath, we observe a reflective layer, locally well stratified and organized. Discontinuous high amplitude reflectors characterize its base, defined in Figure 3a as '*base reflective layer*', and showing small depth variations. From ~150 to ~210 km, top basement is slightly shallower and identified at ~9km depth. Only minor topographic variations are observed except for local highs at top basement (~0.5 sec in height and 5-10 km in width; Fig. 3d). Oceanward, from ~210 to 420 km, top basement is almost flat and characterized by discontinuous high amplitude reflectors. *Seismic Moho* is observable discontinuously as deep reflectors, and appears more clearly on the PSTM profile (Fig. 3a) than on the PSDM one (Fig. 3b). From 0 to 80 km, we define seismic Moho at the base of a reflective package, merging from 80 to 140 km with the interface we identified as the base reflective layer. From ~130 to

210 km, we define seismic Moho at the base of irregular packages of strong reflectors observed between 10 and 11 sec (~15 to 17 km depth) and dipping continentward or oceanward (Fig. 3d). Further oceanward, from ~220 to 420 km, seismic Moho is only locally visible corresponding to a succession of short discontinuous reflectors (Fig. 3a/b).

[Figure 3 about here: Landscape, 2 columns: 204 x 135 mm]

Stratigraphic and basin architecture

We only highlight observations on the first-order stratigraphic and basin architecture. Further detailed descriptions are available in Mangipudi *et al.* 2014 and Haupert *et al.* 2016. From distance 0 to ~80 km, mainly low-β extensional settings are observed. Basement morphology delimits graben and half-graben-type basins and their associated wedge shaped stratigraphic architecture (Haupert *et al.* 2016; Nemčok *et al.* 2013). From ~80 to ~150 km, the oceanward onlapping geometry of the overlaying sediments define the typical passive infill of a post-tectonic sag-sequence (as defined in Masini *et al.* 2013). This sag-sequence is younger than the first sediments onlapping onto oceanic crust (Fig. 3), suggesting that it may still be part of the syn-rift record. As no tectonic deformation is observed in this sequence, it implies that it is post-tectonic. At the base of this post-tectonic sag-sequence, we observe an enigmatic reflective layer that is locally well stratified and characterized by continentward downlaps as observed on the PSTM section, suggesting it may partly correspond to sediments and magmatic flows (Fig. 3c). The apparent occurrence of magmatism at ~110 km prevents further detailed stratigraphic descriptions within this layer. Still, the geometric relationships described within this sequence are compatible with the occurrence of a high-β extensional setting floored by large offset normal faults (i.e. exhumation faults, Fig. 3c) dipping continentward as indicated by the downlapping sediments getting younger in the same direction. This reflective layer was deposited prior to the deposition of post-tectonic sag-sequences and possibly corresponds to syn-exhumation sequences recording the evolution of large offset normal faults. From ~150 to ~420 km, mainly onlaps and passive infill are observed.

Magmatic additions

Magmatic additions seem to be only evidenced in the most distal parts of the SE Indian margin (Fig. 3c/d). From distance 80 to 150 km, spatially delimited, high amplitude reflectors are observed locally crosscutting the overlying stratigraphy, possibly corresponding to sills (planar or saucer shaped morphologies; Planke *et al.* 2005) (Fig. 3c). Similar spatially delimited, high amplitude reflectors are observed within the interpreted basement, some possibly corresponding to sills intrusive in the basement (Fig. 3c). Locally, they show an angular shape similar to the fault block facies unit defined by Planke *et al.* 2005. At about 110 km, the dome shaped topography of the top basement and the associated symmetric downlaps on both sides suggest the occurrence of a presently buried volcanic edifice (~0.8 sec in height and ~30 km in width, Fig. 3c). Its internal structure is not difficult to observe on the seismic profile, but its overall morphology is similar to the 'hyaloclastite mounts' described by Calves *et al.* 2011. Further oceanward from 150 to 210 km (Fig. 3d), the observed local highs at top basement are similar in length and height to the 'outer highs' features described by Calves *et al.* 2011. The paleobathymetry during the emplacement of this volcanic edifice remains, however, difficult to constrain. As the interpreted sills locally crosscut the first sediments of the post-tectonic sag sequence, we suggest that part of the magmatic additions emplaced after the beginning of the passive infill.

Identification of structural domains

Continentward, from distance 0 to ~30 km, accommodation space slightly increases (from 2 to 4 km), locally reaching >5 km within graben and half-graben basins. Continental basement shows little thickness variations (>25 km to ~22 km thick), representative of a *proximal domain* (Fig. 3b). From ~30 to ~80 km, accommodation space progressively increases (from ~4 km to ~9km). The associated deepening of the top basement and ascent of the seismic Moho delimit a progressive extreme thinning of the continental basement from 22 to less than 5 km thick, characteristic of the *thinned domain* (i.e. distal domain of Haupert *et al.* 2016). From ~80 to ~150 km, a large accommodation space is observed (locally >10 km) where we identified the occurrence of a potential high-β extensional setting. We define top basement as the base of the sag-sequence, but suggested the occurrence of syn-exhumation sediments (with a downlapping geometry) and magmatic flows underneath. The nature of the underlying basement cannot be directly constrained but the previously summarized observations are consistent with an *exhumed mantle domain* (see also Haupert *et al.* 2016). Potential field data support the exhumed mantle domain hypothesis as modelled by Nemčok *et al.* (2013). From ~210 km to the end of the line, top basement and seismic Moho are almost parallel and define a ~5 km thick transparent basement characteristic of the *oceanic domain*. The observed thickness of oceanic crust is consistent with regional gravity inversion results in the Bay of Bengal (Radhakrishna *et al.* 2010).

From ~150 to ~210 km, accommodation space is reduced to ~8 km and the top basement and seismic Moho define a 9 to 10 km thick basement (see also Radhakrishna *et al.* 2010; Nemčok *et al.* 2013). Intra-basement reflectivity is frequent (Fig. 3d) dipping oceanward and continentward and often observed underneath the small volcanic edifices presented on Figure 3d. Therefore, this domain differs from the adjacent exhumed mantle and oceanic domains (see also Nemčok *et al.* 2013). The suggested increasing occurrence of magmatic additions towards the oceanward end of the exhumed mantle and the proximity of unambiguous oceanic crust (Fig. 3c/d) are characteristic features of *proto-oceanic domains* at magma-poor rifted margins (Iberia-Newfoundland: Welford *et al.* 2010; Peron-Pinvidic *et al.* 2013; Autralia-Antarctica: Gillard *et al.* 2015). The passage from the exhumed mantle to proto-oceanic domain is transitional highlighted by the progressive step-up morphology of the top basement (from ~10 to ~8 km depth). The passage from the proto-oceanic to oceanic domain appears equally transitional, here marked by an ascent of the Moho and slight deepening of the top basement.

Interpretations and scenarios for the nature of the proto-oceanic domain

General interpretation

Several interpretations have already been presented along this profile (e.g. Nemčok *et al.* 2013; Haupert *et al.* 2016; Pindell *et al.* 2014). The overall architecture presented in this work (Fig. 3 &4) share many similarities with the one of Haupert *et al.* 2016 except within the exhumed mantle domain and oceanward, where we defined the proto-oceanic domain.

The proximal domain is characterized by a weak thinning of the continental crust. We interpret a set of classical normal faults mainly dipping oceanward and delimiting half-graben basins, likely rooting at mid-crustal levels (possibly corresponding to some faint reflectivity observed at about 15 km depth, Fig. 3b). The beginning of the thinned domain coincides with the break-away of a fault system corresponding to a major escarpment at about 30 km (R1 in Haupert *et al.* 2016), associated with a relatively large offset. Conjugate structures may occur at depth structuring the necking of the continental crust (Mohn *et al.* 2012). Further oceanward from 40 to 60 km, we interpret only small rift basins (a few kilometres wide). As the associated faults show a limited offset, they likely root within shallow crustal levels. Another important escarpment is observed at about 60 km (R2 in Haupert *et al.* 2016) where the crust is already thinned to less than 10 km thick. A set of oceanward dipping faults possibly locally offsetting the Moho (Fig. 4) can be interpreted, suggesting that some of these faults can cut through the entire crust, hence likely embrittled. Such faults may allow the serpentinization of the underlying mantle (Pérez-Gussinyé & Reston 2001).

The exhumed mantle domain is characterized by the interpreted occurrence of exhumation faults on top of which, an enigmatic reflective layer was identified and described (Fig. 3). The nature of this reflective layer is uncertain and may correspond to a volcanosedimentary sequence (including both sediments and magmatic flows) consistent with the frequently suggested occurrence of magmatic additions (Fig. 3c). Similar sequences are notably described over the exhumed mantle of the Newfoundland (Peron-Pinvidic *et al.* 2010; Gillard *et al.* 2016b) and Australian-Antarctica rifted margins (Gillard *et al.* 2016b) recording the progressive formation of new basement surfaces along exhumation faults and the associated magmatism. We interpret these exhumation faults to be dipping continentward, consistently with the interpretation of Haupert *et al.* 2016, based on the geometry observed in these syn-tectonic sequences. These exhumation faults are associated with topographic variations (Fig. 3a), possibly corresponding to normal faults crosscutting the previously exhumed basement as suggested from the fault block morphology (Planke *et al.* 2005) of some inferred intrusives (Fig. 3b/c and 4). Magmatism is interpreted to occur within the exhumed mantle domain (Fig. 3c) and seems to become progressively more important toward the proto-oceanic domain as indicated by the increasing occurrence of magmatic intrusives at depth and in the overlying sediments (Fig. 3c). The first oceanic crust likely emplaced at a steady-state spreading system is relatively thin consistently with regional observations in the Bay of Bengal (Radhakrishna *et al.* 2010).

[Figure 4 about here: Portrait, 2 columns: 135 x 204 mm]

Scenarios of the nature of the proto-oceanic domain

This domain is described in a few studies at magma-poor margins (e.g. Jagoutz *et al.* 2007; Welford *et al.* 2010; Bronner *et al.* 2011; Gillard *et al.*, 2015, 2016b, 2017; Peron-Pinvidic *et al.* 2013). Up-to-now, two drill-holes are publically available in similar domains, at the most distal parts of the Iberia-Newfoundland rifted margins (Ocean Drilling Program–ODP, sites 1070 and 1277; Shipboard Scientific Party 1998; 2004). Potential analogues of proto-oceanic domains are identified in remnants of the Alpine Tethys rifted margins (e.g. Chenaillet ophiolite, Manatschal *et al.* 2011; Lower Platta nappe, Desmurs *et al.* 2002). Nevertheless, the nature of the basement, the architecture and magmatic budget of these domains are uncertain and likely vary from one rifted margin to the other (Peron-Pinvidic *et al.* 2013; 2017). Therefore, we prefer presenting different interpretations involving variable magmatic budget rather than one solution.

The local highs observed in the proto-oceanic domain (Fig. 3d) are similar in shape to outer highs commonly interpreted as volcanic edifices near oceanic domains in settings considered as magma-rich (e.g. Planke *et al.* 2000; Calvès *et al.* 2011). This analogy straightforwardly suggests that the proto-oceanic domain could be made of igneous crust only *(scenario 1*, Fig. 4a), locally ~10 km thick (Fig. 3b; Nemčok *et al.* 2013). The intra-basement reflectivity observed underneath could reasonably be interpreted as corresponding to the deep structure of the volcanic edifices and the reflective patterns above seimic Moho as magmatic intrusives (Fig. 3d). Thick igneous crust and volcanic edifices are common in magma-rich rifted margin contexts adjacent to continental crust (Menzies *et al.* 2002; Nielsen & Hopper 2004) as observed for example at the West-Indian rifted margin: (Calvès *et al.* 2011), Hatton Bank, (White *et al.* 2008) or SE Greenland (Larsen *et al.* 1998; Hopper *et al.* 2003). If this interpretation is indeed possible, it is quite surprizing for a rifted margin where adjacent mantle exhumation is inferred and considered to be magma-poor (Nemčok *et al.* 2013; Radhakrishna *et al.* 2012; Sinha *et al.* 2016; Pindell *et al.* 2014; Haupert *et al.* 2016).

Various forms of magmatic additions seem to occur in the interpreted exhumed mantle domain (Fig. 3c). The oceanward limit of potentially exhumed mantle appear gradual and magmatic additions seem to become more important oceanward. Hence, an alternative interpretation for this domain (*scenario 2*, Fig. 4b) could be that the basement is composed of exhumed serpentinized mantle progressively ‘sandwiched’ between magmatic extrusive (basalts?) and intrusive material (gabbroic underplates?). Intra-basement reflectivity could correspond to the top of faulted exhumed mantle, variably intruded (by feeder dikes?), on top of which extrusives and local volcanic edifices can be emplaced. The additional presence of continental crust fragments cannot be excluded (e.g; Nemčok *et al.* 2013). The locally thick reflective packages observed above the interpreted seismic Moho could correspond to sill-like intrusives (gabbroic?) forming a mafic underplated body at the base of serpentinized exhumed mantle. Bronner *et al.* (2011) suggested a similar interpretation at the Iberia-Newfoundland rifted margins based on refraction and reflection seismic data and observations from the ODP Sites 1277 that penetrated exhumed mantle and recovered intrusives and extrusive mafic material (Jagoutz *et al.* 2007). The Chenaillet ophiolite preserved in the Alps (Manatschal *et al.* 2011) can be considered as an analogue of this interpretation of the proto-oceanic domain (Gillard *et al.*, 2015; 2016b). There, basaltic rocks deposited on top of exhumed serpentinized peridotites are exposed (Manatschal *et al.* 2011). These volcanic sequences appear to seal normal faults that developed in the previously exhumed serpentinized mantle (Manatschal *et al.* 2011).

In our last alternative (*scenario 3*, Fig. 4c), we suggest that the reflective packages observed above the interpreted seismic Moho could in fact be within the mantle, possibly corresponding to a layer of magma entrapment. The overall architecture interpreted for the proto-oceanic domain is similar to the *scenario 2* except for a thinner underplated magmatic layer and the suggested presence of melt entrapment within the mantle. The occurrence of melt impregnation and stagnation within lithospheric mantle is documented at the most distal parts of present-day rifted margins based on drilling results (Iberia-Newfoundland, Muntener & Manatschal 2006). Similar observations are made in onshore fossil analogues of exhumed mantle and embryonic oceanic domains preserved in the Alps (Muntener & Piccardo 2003; Munterner *et al.* 2004; Muntener *et al.* 2010; Picazo *et al.* 2017).

Uruguay rifted margin case example

Geological setting and first-order tectono-magmatic context

The Brazilian, Uruguayan and Argentinian rifted margins of South America (including the Pelotas, Salado and Colorado basins, Fig. 2) were initially conjugate to the Namibian and South-African rifted margins through the Walvis, Lüderitz and Orange Basins (e.g. Rabinowitz & LaBrecque 1979; Gladczenko *et al.* 1997; Blaich *et al.* 2011; Heine *et al.* 2013; Moulin *et al.* 2010; Torsvik *et al.* 2009). The South Atlantic rifted margins result from the Late Jurassic-Early Cretaceous breakup of West Gondwana (e.g. Rabinowitz & LaBrecque 1979; Gladczenko *et al.* 1997; Heine *et al.* 2013; Moulin *et al.* 2010; Torsvik *et al.* 2009; Frizon De Lamotte *et al.* 2015). In between the Rio Grande and Falkland-Agulhas fracture zones, onset of rifting occurred in the latest Jurassic (e.g. Heine *et al.* 2013 and references therein). A first rift event is associated with the formation of several rift basins trending NW-SE, obliquely to the final margin structure such as the Salado/Punta del Este (e.g. Stoakes *et al.* 1991; Soto *et al.* 2011) and Colorado (Autin *et al.* 2013) basins (Fig. 2). Then, the formation of the South Atlantic and onset of oceanic spreading occurred diachronously related to a progressive and segmented propagation from south to north (e.g. Franke *et al.* 2007; Franke 2013; Koopmann *et al.* 2014; Blaich *et al.* 2013; Heine *et al.* 2013; Stica *et al.* 2014 and references therein) between ~137 to 126 Ma.

In the South Atlantic Ocean, the Rio Grande Rise and Walvis Ridge are generally interpreted to mark the passage of the Tristan Da Cunha hotspot (Fig. 2) responsible for the eruption of the Paraná-Etendeka Large Igneous Province (LIP) (Gibson *et al.* 2006) between 138 and 129 Ma (Peate 1997; Stewart *et al.* 1996; Turner *et al.* 1994). The relationship between LIP emplacement and rifting is complex and the detailed spatial and temporal relationship remains unclear (Franke *et al.* 2007; Franke 2013; Stica *et al.* 2014; Frizon De Lamotte *et al.* 2015). This complexity may partially be explained by the progressive and segmented northward propagation of the South Atlantic prior to and during the emplacement of the Paraná-Etendeka

LIP (Franke *et al.* 2007; Koopmann *et al.* 2014). As a result, the Paraná-Etendeka LIP can be considered as pre-, syn- or post-rift depending on the margin segment considered (Stica *et al.* 2014).

We focus on a high-resolution reflection seismic profile provided by ION Geophysical, striking NW-SE offshore Uruguay across the Salado/Punta del Este basin and terminating in the South Atlantic Ocean (Fig. 2). The Uruguay rifted margin, as most margins of the southern South Atlantic, shows thick SDR sequences (Franke *et al.* 2007; Soto *et al.* 2011; Clerc *et al.* 2015) considered as characteristic of magma-rich rifted margins (Hinz 1981; Mutter 1985; Planke *et al.* 2000; Menzies *et al.* 2002; Lundin & Doré 2015).

Seismic observations

First order interfaces

Seafloor progressively deepens from less than 500 m continentward to more than 4 km at the oceanward end of the profile in the South Atlantic Ocean (Fig. 5). From distance 0 to ~140 km, *top basement* is defined at the top of a reflective package, locally showing evidence of erosional truncations (e.g. near 40 km; Fig. 5). It corresponds to the interface between the base passive infill (from 0 to ~80 km) or base syn-rift (from 80 to 120 km) and acoustic basement (including either pre-rift and magmatic sequences, or crystalline basement; Stoakes *et al.* 1991). It progressively deepens from ~1.5 to ~4 km and is characterized by local topographic variations (between ~80 and ~120 km). From ~140 to ~240 km, top basement is only characterized by faint local reflections. We define it at the base of syn-rift sediments where observable (Fig. 5c). From 240 km to the end of the profile, high amplitude reflectors at the top of SDRs and at the base of passive infill characterize the top basement oceanward (Fig. 5d), corresponding to an almost flat interface. From ~260 to ~340 km, we tentatively define the *base of SDRs*. From 260 to 280 km, it corresponds to a relatively well-defined high amplitude reflector, at the base of the SDR package. From ~290 to ~340 km, we define it at the downward termination of SDRs (Fig. 5d). Along the profile, deep reflectors are commonly observed and interpreted as s*eismic Moho.* They are notably well imaged on the PSTM profile (Fig. 5a). From 0 to 80 km, from ~150 to ~210 km, and from ~260 to 310 km, we define seismic Moho at the base of parallel discontinuous high amplitude reflectors commonly forming packages locally more than 1 sec thick (~5 km thick). Further oceanward, from ~320 km to the end, seismic Moho corresponds to a succession of short parallel discontinuous reflectors.

[Figure 5 about here: Landscape, 2 columns: 204 x 135 mm]

Stratigraphic and basin architecture

From distance 0 to ~260 km, basement morphology defines graben and half-graben-type basins corresponding to low-β extensional settings. Still, these basins are locally quite deep (~12-13 km depth), associated with the relatively thick rift sequences of the Punta del Este basin (locally more than 6-7 km thick, Fig. 5, Stoakes *et al.* 1991). Symmetric onlaps of sedimentary sequences are more commonly observed than typical wedge-shaped geometries (Fig. 5a). From 260 to 380 km, we observe continentward onlaps onto top basement marking a progressive post-SDRs emplacement continentward passive infill (Fig. 5a/d). From 380 km to the end of the line, oceanward downlaps can be observed (Fig. 5a).

Magmatic additions

Continentward, from distance 120 to 260 km, magmatic additions are suggested to occur mainly as sill-like intrusives into sedimentary sequences of graben and half-graben-type basins (Fig. 5). Sills appear as spatially limited high amplitude reflectors either parallel to or crosscutting the stratigraphy corresponding to 'planar', 'planar transgressive', and 'saucer-shaped' morphologies (Planke *et al.* (2005) (e.g. at 150 km). Evidence of magmatism is interpreted at ~220 km (Fig. 5c). The overall dome shaped morphology, with roughly symmetric flanks is characteristic of a volcanic edifice, possibly also associated to sill intrusions. Interestingly, this volcanic edifice appears to be sitting on top of syn-rift and possible early post-rift sequences, suggesting that magmatic activity mainly occurred after the formation of graben–type basins. The exact onset and timing remains nevertheless difficult to constrain in more detail. From ~260 to ~380 km, we observe SDRs characterized by high amplitude reflectors terminating rather abruptly at depth. SDRs are classically interpreted as volcanic flows (Hinz 1981; Mutter *et al.* 1982) emplaced in sub-aerial to shallow conditions based on drilling results e.g. off Norway (Eldholm *et al.* 1987; 1989) and SE Greenland (Larsen *et al.* 1994; Larsen & Saunders1998; Duncan *et al.* 1996). To first-order, the most continentward SDR sequence has a wedge shaped geometry. Further oceanward (Fig. 5d) the SDR sequences correspond to a succession of nearly parallel reflections, whereas further oceanward, they show again a clear wedge shaped geometry. From ~320 to ~340 km, we observe a progressive decrease in the length of these SDRs. From ~340 to ~360 km, we observe local high amplitude reflectors (mainly observable on the PSTM section) dipping oceanward, still possibly corresponding to short SDR sequences. At their base, we identify weak horizontal discontinuous reflectors.

Magmatic additions at the base or within the basement are also likely but remain difficult to identify unambiguously. We note that where we identified potential sill intrusions and volcanic buildups into rift basins, the base of the crust defining seismic Moho, is often ill defined. This observation contrasts with the relative ubiquitous occurrence of high amplitude discontinuous parallel reflectors at the base of the crust along the profile. Some of these deep reflective packages are observed oceanward (~240 to ~370 km; Fig. 5). They may partly correspond to intrusive magmatic bodies emplaced at the base of the crust synchronously with the SDR sequences.

Identification of structural domains

Continentward, from distance 0 to ~140 km, accommodation space slightly increases from ~1.5 to ~3.5 km, locally reaching a maximum of 5 km within a graben-type basin (Fig. 5). Top basement and seismic Moho are almost parallel and flat, defining an approximately 25 to 30 km thick continental basement, consistent with the occurrence of a *proximal domain*. From ~140 to ~260 km, evidence for locally deep graben and half-graben basins are identified, associated with a progressive important increase in accommodation space oceanward (from ~3.5 to ~7.5 km, locally >12km). The progressive deepening of top basement and Moho depth variations reflect crustal thickness variations from 25 km to possibly locally less than 15 km (at about 220 km), characteristic for a *thinned domain*. Magmatism is evidenced in this domain possibly occurring during early post-rift time. From 380 km to the end of the line, top basement and Moho are roughly parallel, defining a 6 to 7 km thick transparent basement, except for the local occurrence of internal reflectors, characteristic of the *oceanic domain*.

From 260 to 320 km, accommodation space show only little increase oceanward (from 7 to 8 km), as the top basement remains relatively flat. In contrast, at depth, seismic Moho variations define a “crustal keel” locally delimiting a 20 km thick basement continentward, getting progressively thinner oceanward (from ~310 to ~380 km). SDRs are observed at the base of passive infill, below top basement (as defined in this work), and becoming thicker oceanward, as suggested by the base of SDRs geometry (Fig. 5d). Associated intrusions possibly also occur at the base of the crust (Fig. 5). The occurrence of SDRs and proximity of standard oceanic crust (~7 km thick, White *et al.* 1992) are characteristic features of ‘continent-ocean transitions’ (COT), ‘transitional crust’ or ‘outer domains’ at magma-rich rifted margins, (Franke 2013; Menzies *et al.* 2002; Peron-Pinvidic *et al.* 2013), referred to in this work as *proto-oceanic domain.* A deepening of Moho reflections (from ~240 to ~270) marks the transition from the thinned to proto-oceanic domain, while top basement remains flat. The transition from our defined proto-oceanic domain to a standard oceanic domain possibly occurs where an inflection in seismic Moho topography is observed.

Interpretation and scenarios for the nature of the proto-oceanic domain

General interpretation

Interpretations of the overall rifted margin architecture were previously published based on adjacent lines and other seismic surveys (e.g. Franke *et al.* 2007; Soto *et al.* 2011; Clerc *et al.* 2015) sharing some similarities with the architecture interpreted in this work (Fig. 6). The proximal domain shows a weak thinning of the continental crust consistently with the occurrence of shallow graben-type basins. The transition to the thinned domain is defined where we interpret the breakaway of an important fault delimiting one side of a roughly symmetric deep graben. The overall architecture of our interpreted thinned domain is atypical. This is possibly related to the fact that the profile crosses the Punta del Este basin oriented obliquely (NW-SE) to the final rifted margin segmentation (Soto *et al.* 2011), explaining why this domain is not observed on adjacent profiles located further north (Clerc *et al.* 2015). Local evidence of magmatism is interpreted within this domain corresponding to sill complexes, a volcanic edifice, and possible intrusions at depth (Fig. 5). The transition from the thinned to proto-oceanic domain is interpreted as gradual, approximately at the continentward end of the first SDR sequences. Similarly, the passage from proto-oceanic to oceanic appears transitional. The first oceanic crust likely emplaced at a steady-state spreading system is 6 to 7 km thick, consistent with global average (~7±1 km, White *et al.* 1992).

[Figure 6 about here: Portrait, 2 columns: 135 x 204 mm]

Scenarios of the nature of the proto-oceanic domain

Most studies at magma-rich rifted margins place the COT, ie. our proto-oceanic domain, where SDRs occur, either at their landward/seaward edge, or in the center (Franke 2013). Several legs of the Deep Sea Drilling Project–DSDP and ODP drilled SDR sequences off the British Isles (leg 81, Roberts *et al.* 1984), offshore Norway (leg 104; Eldholm *et al.* 1987), and SE Greenland (legs 152, Larsen *et al.* 1994; and 163, Duncan *et al.* 1996). Drilling results confirmed the volcanic nature of SDRs, interweaved with some sediments and the geochemical signatures of the lava flows showed a decrease in continental contamination oceanward (Larsen & Saunders 1998; Saunders *et al.* 1998). Even if they may not use the same terminology as the one used in this work, many studies focused on this domain (e.g. Hinz 1981; Mutter 1985; Gladczenko *et al.* 1997; Planke *et al.* 2000; Franke *et al.* 2010). Most debates are related to the emplacement mechanism related to the formation of SDRs (e.g. Larsen & Saunders 1998; Franke *et al.* 2010; Paton *et al.* 2017; Buck 2017) and on the nature of the underlying basement (e.g. Larsen *et al.* 1998; Hopper *et al.* 2003; Geoffroy 2005; Geoffroy *et al.* 2015). In the following, we present different interpretations for the nature and architecture of the proto-oceanic domain involving variable magmatic budget that are compatible with our seismic observations.

The first SDR package observed shows a wedge shaped geometry, suggesting a fault controlled geometry. Over this first sequence, SDRs appear sub-parallel 'prograding' oceanward, suggesting a minor role of faulting, consistent with a proto-oceanic domain made of igneous crust only (*scenario 1*; Fig. 6a), locally ~20 km thick (considering a vertical section between top basement and seismic Moho). In this interpretation, we consider that the continental crust terminates abruptly at the downward termination of the first sub-parallel SDRs (Fig. 5d). The abrupt termination of the continental crust related to the emplacement of thick igneous crust along the proto-breakup axis is inspired from studies offshore SE Greenland (Larsen *et al.* 1998; Larsen & Saunders 1998; Hopper *et al.* 2003); Hatton Bank (White *et al.* 2008) and Norway (Eldholm *et al.* 1987) where SDRs were drilled. The deep reflective packages observed above the interpreted seismic Moho could then be interpreted as the intrusive equivalent of SDRs, possibly corresponding to mafic underplates (Skogseid *et al.* 2000; White *et al.* 2008).

The wedge shaped geometries of the most continentward and oceanward SDRs suggest a possible syn-magmatic fault activity consistent with a proto-oceanic domain including thin continental crust getting more and more intruded oceanward (*scenario 2*, Fig. 6b). Intruded continental crust remnants are interpreted as sandwiched between SDRs and magmatic underplates at depth. This intruded basement is commonly referred to as 'transitional crust' (e.g. Franke *et al.* 2010; Franke 2013; Abdelmalak *et al.* 2015; Geoffroy *et al.* 2015; Geoffroy 2005). The base of the SDR sequences (Fig. 5) could then indicate the top of the intruded continental crust. The deep reflective packages at depth (Fig. 5) could correspond to intruded lower crust (Geoffroy *et al.* 2015) or to mafic underplates referred to as Lower Crustal Body–LCB (Gernigon *et al.* 2006). Field observations from suggested fossil analogues preserved in the Scandinavian Caledonides (Abdelmalak *et al.* 2015) show complex dike generations intruding a continental basement. Evidence for complex and polyphase syn-magmatic fault activity is documented in Afar (Geoffroy *et al.* 2014; Stab *et al.* 2016). The hypothesis of fault controlled emplacement of SDRs is commonly suggested at present-day magma-rich rifted margins of the South Atlantic (e.g. Geoffroy *et al.* 2015; Franke *et al.*, 2010, 2007; Stica *et al.* 2014; Becker *et al.* 2016).

In our last alternative interpretation, we suggest that the deep reflective packages observed at depth could be within the mantle (*Scenario 3*, Fig. 6c). The overall architecture of the proto-oceanic domain is interpreted to be similar to scenario 2 except for a thinner layer of underplated material and the suggested occurrence of melt bodies trapped within the mantle. Geochemical studies from the Main Ethiopian Rift considered as a tectonically active analogue of a magma-rich setting show a complex and protracted magmatic evolution associated with melt stagnation levels within the lithospheric mantle (Rooney *et al.* 2014; 2017).

Identifying the timing and amount of magmatic additions

Interpretations derived from seismic reflection data are non-unique and therefore imply significant uncertainties when it comes to suggesting geological interpretations. On the one hand, determining the precise timing of magma emplacement is problematic and can only be done for extrusives, based on relationships with the stratigraphy (Fig. 3c; Fig. 5c). On the other hand, the identification of magmatic additions and in particular magmatic intrusives within crystalline basement is difficult to constrain as both rock types often share similar petrophysical properties (densities/velocities). In the absence of drill-hole data, based on seismic reflection data only, resolving the precise timing and exact volume of magmatic additions remains challenging.

Indirect determination of the timing of magma emplacement

On the Uruguay rifted margin, our observations suggest that most of the magmatism was emplaced early after the rifting phase related to the formation of the Salado/Punta del Este Basin (Fig. 5c), consistent with observations reported by regional studies (e.g. Heine *et al.* 2013). As SDR sequences, most likely corresponding to lava flows, progressively develop into unambiguous standard oceanic crust (7±1 km, White *et al.* 1992), we can suggest that they were emplaced at lithospheric breakup. Intrusives likely occur at the base of the crust (Fig. 5). The timing of emplacement cannot be ascertained but the proximity of SDRs suggest that they may be similar to the distal magmatic intrusions (LCB) interpreted as related to lithospheric breakup in the Colorado Basin further south (Autin *et al.* 2016).

On the SE-Indian rifted margin, magmatic additions are suggested to occur only in the ultra-distal parts and in continuity with the first unequivocal oceanic domain (Fig. 3). Part of the magmatic additions possibly emplaced during or early after mantle exhumation as indicated by the inferred occurrence of a volcanic edifice on top of possible syn-tectonic sequences (reflective layer, Fig. 3c). Part of the magmatism likely emplaced after the deposition of the post-tectonic sag-sequences, ie. after the onset of the passive infill, as indicated by the likely presence of sill-like intrusions crosscutting the overlaying stratigraphy (Fig. 3c). Based on these deductions, we believe that most of the magmatism observed is likely to be part of lithospheric breakup processes.

Uncertainties in determining the magmatic budget

The identification of magmatic extrusives (volcanic edifices, SDRs) can reasonably be done based on our high-resolution PSTM and PSDM seismic reflection data. However, determining the overall magmatic budget and notably the amount of distal magmatic additions intrusive at the base or within basement remains challenging. High resolution refraction data may help distinguish between pre-rift lower crust and intrusives emplaced at lithospheric breakup as shown from the Hatton Bank example (White *et al.* 2008). Integrated quantitative approaches can be used to examine the shape (Skogseid *et al.* 2000; Autin *et al.* 2013) and nature (Nirrengarten *et al*. 2014; Autin *et al*. 2016) of distal LCB characteristic of magma-rich rifted margins. Potential field modelling represents a useful tool to test different interpretations and to provide quantitative verifications that could narrow down the number of possible solutions. Nevertheless, they cannot provide unique solutions as different lithologies may present similar geophysical properties (Christensen & Mooney 1995). In addition, the intense tectonic and/or magmatic activity affecting the distal domains of rifted margins strongly alter the initial petrophysical proprieties of the rocks that form these domains. As a result, the average density and velocity used as input for forward modelling would in fact be very similar between our different scenarios (Péron-Pinvidic *et al.* 2016).

Because of these uncertainties, we decided to present and discuss three alternative interpretations for each of our two case examples (Fig. 4&6). The hypotheses for the architectures of proto-oceanic domains result in different scenarios for the magmatic budget at lithospheric breakup. As these interpretations are compatible with the limited drilling results in offshore analogues (where available) and/or with onshore field observations previously described, we believe that all of them can be considered as geologically coherent and plausible. These interpretations represent non-unique 'end-member' scenarios based on which we aim to discuss fundamental processes related to lithospheric breakup at rifted margins whether they are considered as representative of magma-poor or magma-rich archetypes.

Magmatic budget at rifted margins: discussion

Architecture of proto-oceanic domains and implications for lithospheric breakup processes

Based on the interpretations of the proto-oceanic domain architecture previously suggested for the SE-Indian and Uruguayan rifted margins (Fig. 4 and 6), we first examine and tentatively estimate the magmatic budget at lithospheric breakup for each scenario (Fig. 7). Secondly, based on the inferred evolution of melt production in the proto-oceanic domain, we present different potential mechanisms for lithospheric breakup involving different tectono-magmatic interactions (Fig. 7&8).

[Figure 7 about here: Landscape: 204 x 135 mm]

[Figure 8 about here: Portrait, 2 columns: 135 x 204 mm]

In *scenarios 1*, whether we consider the SE-Indian or the Uruguayan rifted margin, the proto-oceanic domain is suggested to be dominantly made of igneous crust, respectively reaching ~10 and ~20 km thick. In both cases, the thickness of magmatic additions exceeds the 7±1 km standard thickness (Fig. 7; White *et al.* 1992; Brown & White 1994) predicted from decompression melting models (White & McKenzie 1989). The volume of magmatic additions is reduced to standard thicknesses in the oceanic domain (Fig. 7), even less in the case of SE-India. The clear increase in magmatic additions suggested in the proto-oceanic domain of the scenarios 1 is consistent with a relatively fast melt production at lithospheric breakup that would appear rather 'instantaneous' at a geological scale (Fig. 8). This excess magmatic event/pulse is transient and often advocated to occur at the rift to drift transition of magma-rich rifted margin (Nielsen & Hopper 2004). Nevertheless, the possibility of an excess magmatic event/magmatic pulse at lithospheric breakup has also been considered in the case of the Iberia-Newfoundland rifted margins, archetype of magma-poor settings (Bronner *et al.* 2011).

In *scenarios 2*, the proto-oceanic domain corresponds to a complex basement respectively composed of intruded exhumed serpentinized mantle (SE-India) or intruded continental crust (Uruguay) sandwiched in-between extrusive and intrusive material. As a result, in both cases, the apparent total crustal thickness (ie. between top basement and seismic Moho, Figs. 3&5) is due to the cumulative effect of magmatic additions and continental crust/exhumed serpentinized mantle thicknesses (Fig. 7). Interestingly, magmatic addition thickness is strongly reduced compared to scenarios 1 and does not necessarily exceed the 7±1 km standard thickness (White *et al.* 1992; Brown & White 1994) derived from decompression melting model predictions (White & McKenzie 1989). As a result, in both cases, a relative progressive increase in melt production can be suggested at lithospheric breakup that may appear ‘gradual’ (Fig. 8; Whitmarsh *et al.* 2001a), possibly recorded within wide areas (e.g. Gillard *et al.* 2015). Extensional tectonic processes (mechanical thinning) are likely dominant in the initial stages of lithospheric breakup either related to polyphase extensional deformation within exhumed mantle domain at magma-poor rifted margins (Gillard *et al.* 2016a, 2016b) or to explain the formation of SDRs at magma-rich rifted margins (e.g. Franke *et al.* 2010, 2007). Magmatic processes become more important only towards the end of lithospheric breakup (Peron-Pinvidic & Osmundsen 2016; Gillard *et al.* 2015, 2017).

In *scenarios 3*, the architectures suggested for the proto-oceanic domain are similar to the ones presented in the scenarios 2 except for the presence of melt stagnation levels within the mantle. The amount of remnants of continental crust/exhumed serpentinized mantle in between igneous material and the volume of melt entrapped in the mantle is difficult to estimate (Fig. 7). However, as suggested for the scenarios 2, magmatic addition thickness does not necessarily exceed the 7±1 km standard thickness (White *et al.* 1992; Brown & White 1994) derived from decompression melting model predictions (White & McKenzie 1989) even for the Uruguayan case example. In both cases, the interpreted occurrence of melt entrapment implies an inefficient/incomplete extraction of melt out of the mantle possibly suggesting variable melt production resulting in a polyphase or ‘stuttering’ (Jagoutz *et al.* 2007) lithospheric breakup (Fig. 8). Such lithospheric breakup processes are likely to be associated to important local variations in the magmatic budget comparable to what is observed in present-day ultra-slow spreading systems (Cannat *et al.* 2008; Sauter *et al.* 2016), often used as analogues to understand COT (Cannat *et al.* 2009; Pérez-Gussinyé *et al.* 2006). The Main Ethiopian Rift may correspond to a nascent analogue, where the transition from mechanical/tectonic-dominated to magmatic-dominated processes appear as largely spatially distributed and temporally protracted (Rooney *et al.* 2014).

Some implications for the reappraisal of magma-poor versus magma-rich rifted margin archetypes

Despite different volumes of magmatism, we presented several potential mechanisms for lithospheric breakup applicable to both magma-poor and magma-rich archetypes related to different melt production and tectono-magmatic interplays (Fig. 7&8). The Uruguayan and other rifted margins showing magma-rich morphologies may be explained by excess decompression melting compared with steady-state seafloor spreading (scenario 1, Fig 7&8) but could also involve a monotonic (scenarios 2&3, Fig 7&8) increase in decompression melting with an early onset relative to crustal breakup. The converse, where the onset of decompression melting occurs later relative to crustal breakup allows for mantle exhumation characterizing magma-poor rifted margin. The transition from exhumed mantle to oceanic crust at the SE-Indian and other rifted margins showing magma-poor characteristics could result from an excess decompression melting event compared with steady-state seafloor spreading (scenario 1, Fig 7&8). This contrasts with the progressive (scenario 2, Fig 7&8) or 'stuttering' (scenario 3, Fig 7&8) onset of decompression melting (Whitmarsh *et al.* 2001a; Jagoutz *et al.* 2007) more classically inferred. As a result, we highlight that the formation of each archetype (magma-poor or magma-rich) could result from different tectono-magmatic interactions and melt production at lithospheric breakup. Davis & Lavier (2017) draw a similar conclusion based on numerical simulations, showing that several variables can lead to the formation of an end-member archetype morphology.

To account for the uncertainty in determining the magmatic budget at rifted margins and notably the amount of underplated material, we presented three interpretations for each case study. A notable difference for all interpretations between the SE-Indian/magma-poor and Uruguayan/magma-rich case example is related to the onset of decompression melting relative to the amount of crustal thinning (rift evolution). The timing of decompression melting onset relative to crustal thinning appears to be as an important parameter to consider, equal to, if not more important than the magmatic budget to understand the processes occurring at the rift-to-drift transition and the worldwide variability of rifted margins.

Parameters controlling melt production and onset of decompression melting: area for further research

Several studies have focused on the parameters controlling the onset of decompression melting and the amount of melt production at rifted margins (e.g. Nielsen & Hopper 2004; Pérez-Gussinyé *et al.* 2006; Minshull *et al.* 2001; Fletcher et al. *et al.* 2009; Armitage *et al.* 2010; Lundin *et al.* 2014; Davis & Lavier 2017). They notably revealed the importance of mantle temperature, extension rates, mantle composition, preceding rift history (inheritance) and absence or occurrence of active upwelling of the asthenosphere. Mantle temperature is classically considered to represent one of the main factors controlling the onset of decompression melting and the magmatic budget (e.g. White & McKenzie, 1989). Elevated mantle temperatures enhance melt supply and are often considered as the main parameter controlling the magmatic budget at magma-rich rifted margins (e.g. Skogseid *et al.* 2000). In contrast, lower mantle temperatures inhibit and delay decompression melting onset. Extension rates at lithospheric breakup are also considered to have a significant effect on magma supply (Lundin *et al.* 2014). Lundin *et al.* 2014 notably suggested that magma-poor/magma-rich settings are mainly determined by the opening rate of regional tectonic plates and distance to the associated Euler pole. Mantle composition is also known to control melt production: the more primitive and volatile-rich the mantle is, the more melt it may produce and vice versa, if the mantle is depleted (Cannat *et al.* 2009). Melt extraction efficiency (Muntener *et al.* 2010), rift-induced processes such as melt infiltration and stagnation resulting from melt-rock reactions within lithospheric mantle (Muntener *et al.* 2004; Picazo *et al.* 2017) appear also important.

In detail, the magmatic budget and formation of end-member archetypes is likely controlled by a complex interaction between these parameters (e.g. Pérez-Gussinyé *et al.* 2006; Fletcher *et al.* 2009; Armitage *et al.* 2010; Brown & Lesher 2014; Davis & Lavier 2017). Based on numerical simulations, Pérez-Gussinyé *et al.* 2006 showed that a decrease in melt production cannot solely be a function of extension rates requesting an additional key role of mantle temperature or composition. Some studies reveal the role on the magmatic budget of the timing of a mantle thermal anomaly emplacement relative to the rift evolution (Skogseid *et al.* 2000; Armitage *et al.* 2010). Further work is required to better unravel the interplay of parameters controlling the timing and amount of melt production as well as to determine more precisely its volume in seismic sections.

Conclusions

Based on a number of morphological features, rifted margins are commonly defined as either ‘magma-poor’ or ‘magma-rich’ (e.g. Sawyer *et al.* 2007; Reston 2009; Reston & Manatschal 2011; Franke *et al.* 2013; Doré & Lundin 2015). This terminology/classification results in assumptions on the magmatic budget of rifted margins during rifting and at lithospheric breakup. In this work, we re-appraised and questioned a presently prevailing model that magma-rich margins necessarily have excess decompression melting during lithospheric breakup compared with steady-state seafloor spreading and that magma-poor margins have inhibited melting.

We first highlighted the difficulty in resolving the magmatic budget at rifted margins based on seismic reflection data only. Quantitative analyses could be used to narrow down the number of potential hypotheses but would still provide non-unique solutions. To account for this uncertainty, we presented several interpretations, each supported by onshore field analogues and drilling results in similar settings, where available. As a result, we suggested several mechanisms to achieve lithospheric breakup for each end-member archetype, implying different tectono-magmatic interactions and melt production (scenarios 1, 2 and 3). We showed that the Uruguayan and other magma-rich rifted margins could result from excess decompression melting compared with steady-state seafloor spreading but could also be explained by a gradual or stuttering increase with an early onset relative to crustal breakup (ie. rupture and separation of continental crust). The converse, where the onset of decompression melting is late relative to crustal breakup allows for mantle exhumation, characteristic of the magma-poor rifted margin archetype such as the SE-Indian rifted margin.

Eventually, we show that different tectono-magmatic interactions and melt production can lead to the formation of magma-poor or magma-rich morphologies. In spite of different volumes of magmatism, the lithospheric breakup mechanisms suggested are comparable between magma-poor and magma-rich archetypes. Considerations on the timing of decompression melting onset relative to crustal thinning may be more important than the overall magmatic budget to unravel the processes occurring at the rift-to-drift transition and the worldwide variability of rifted margins.

ACKNOWLEDGMENTS

The authors acknowledge ION Geophysical for providing the two seismic profiles presented in this work. This paper largely benefited from the critical and constructive reviews of Erik Lundin and Tony Doré and additional comments from the editor James A. Hammerstein. We thank the developers of the free software QGis. The MM4 consortium (BP, Conoco Phillips, Statoil, Petrobras, Total, Shell, BHP-Billiton, and BG) financially supported this project. We are grateful to Jakob Skogseid and Philippe Werner for fruitful discussions.

REFERENCES

ABDELMALAK, M.M., ANDERSEN, T.B., ET AL. 2015. The ocean-continent transition in the mid-Norwegian margin: Insight from seismic data and an onshore Caledonian field analogue. *Geology*, **43**, G37086.1, doi: 10.1130/G37086.1.

AMANTE, C. & EAKINS, B.W. 2009. ETOPO1 1 Arc-Minute Global Relief Model: Procedures, Data Sources and Analysis. *In*: NOAA Technical Memorandum NESDIS NGDC-24 (ed.). National Geophysical Data Center, NOAA, 19., doi: 10.7289/V5C8276M.

ARMITAGE, J.J., COLLIER, J.S. & MINSHULL, T.A. 2010. The importance of rift history for volcanic margin formation. *Nature*, **465**, 913–917, doi: 10.1038/nature09063.

ARMITAGE, J.J., COLLIER, J.S., MINSHULL, T.A. & HENSTOCK, T.J. 2012. Thin oceanic crust and flood basalts: India-Seychelles breakup. *Geochemistry, Geophysics, Geosystems*, **12**, 1–25, doi: 10.1029/2010GC003316

AUTIN, J., SCHECK-WENDEROTH, M., ET AL. 2013. Colorado Basin 3D structure and evolution, Argentine passive margin. *Tectonophysics*, **604**, 264–279, doi: 10.1016/j.tecto.2013.05.019.

Autin, J., Scheck-Wenderoth, M., Götze, H.J., Reichert, C. & Marchal, D. 2016. Deep structure of the Argentine margin inferred from 3D gravity and temperature modelling, Colorado Basin. *Tectonophysics*, **676**, 198–210, doi: 10.1016/j.tecto.2015.11.023.

Baksi, A.K., Barman, T.R., Paul, D.K. & Farrar, E. 1987. Widespread early Cretaceous flood basalt volcanism in eastern india: Geochemical data from the Rajmahal-Bengal-Sylhet Traps. *Chemical Geology*, **63**, 133–141, doi: 10.1016/0009-2541(87)90080-5.

Becker, K., Tanner, D.C., Franke, D. & Krawczyk, C.M. 2016. Fault-controlled lithospheric detachment of the volcanic southern South Atlantic rift. *Geochemistry, Geophysics, Geosystems*, **17**, 887–894, doi: 10.1002/2015GC006081.

Belgarde, C., Manatschal, G., Kusznir, N., Scarselli, S. & Ruder, M. 2015. Rift Processes in the Westralian Superbasin , North West Shelf , Australia : Insights From 2D Deep Reflection Seismic Interpretation and Potential Fields Modeling. *In*: *APPEA Conference 2015*. Melbourne, Australian Petroleum Production & Exploration Association, 1–8.

Blaich, O.A., Faleide, J.I. & Tsikalas, F. 2011. Crustal breakup and continent-ocean transition at South Atlantic conjugate margins. *Journal of Geophysical Research: Solid Earth*, **116**, 1–38, doi: 10.1029/2010JB007686.

Blaich, O. a, Faleide, J.I., Tsikalas, F., Gordon, a C. & Mohriak, W. 2013. Crustal-scale architecture and segmentation of the South Atlantic volcanic margin. *In:* Mohriak, W. U., Danforth, A., Post, P. J., Brown, D. E., Tari, G. C., Nemčok, M., & Sinha, S. T. (eds) Conjugate Divergent Margins. *Geological Society, London, Special Publications*, **369**, 167–183, doi: 10.1144/SP369.22.

Boillot, G. & Coulon, C. 1998. *La Déchirure Continentale et L'ouverture Océanique: Géologie Des Marges Passives*. Amsterdam, Gordon and Breach Science Publishers.

Bown, J.W. & White, R.S. 1994. Variation with spreading rate of oceanic crustal thickness and geochemistry. *Earth and Planetary Science Letters*, **121**, 435–449, doi: 10.1016/0012-821X(94)90082-5.

Bronner, A., Sauter, D., Manatschal, G., Péron-pinvidic, G. & Munschy, M. 2011. Magmatic breakup as an explanation for magnetic anomalies at magma-poor rifted margins. *Nature Geoscience*, **4**, 549–553, doi: 10.1038/nphys1201.

Brown, E.L. & Lesher, C.E. 2014. North Atlantic magmatism controlled by temperature, mantle composition and buoyancy. *Nature Geoscience*, **7**, 820–824, doi: 10.1038/ngeo2264.

Buck, W.R. 2017. The role of magmatic loads and rift jumps in generating seaward dipping reflectors on volcanic rifted margins. *Earth and Planetary Science Letters*, **466**, 62–69, doi: 10.1016/j.epsl.2017.02.041.

Callot, J.P., Grigné, C., Geoffroy, L. & Brun, J.P. 2001. Development of volcanic passive margins: Two-dimensional laboratory models. *Tectonics*, **20**, 148–159, doi: 10.1029/2000TC900030.

Calvès, G., Schwab, A.M., et al. 2011. Seismic volcanostratigraphy of the western Indian rifted margin: The pre-Deccan igneous province. *Journal of Geophysical Research: Solid Earth*, **116**, doi: 10.1029/2010JB000862.

Cannat, M. 1996. How thick is the magmatic crust at slow spreading oceanic ridges? *Journal of Geophysical Research: Solid Earth*, **101**, 2847–2857, doi: 10.1029/95JB03116.

Cannat, M., Sauter, D., Bezos, A., Meyzen, C., Humler, E. & Le Rigoleur, M. 2008. Spreading rate, spreading obliquity, and melt supply at the ultraslow spreading Southwest

Indian Ridge. *Geochemistry, Geophysics, Geosystems*, **9**, n/a-n/a, doi: 10.1029/2007GC001676.

Cannat, M., Manatschal, G., Sauter, D. & Péron-Pinvidic, G. 2009. Assessing the conditions of continental breakup at magma-poor rifted margins: What can we learn from slow spreading mid-ocean ridges? *Comptes Rendus Geoscience*, **341**, 406–427, doi: 10.1016/j.crte.2009.01.005.

Choudhuri, M., Nemèok, M., Stuart, C., Welker, C., Sinha, S.T. & Bird, D. 2014. 85°E Ridge, India — constraints on its development and architecture. *Journal of the Geological Society of India*, **84**, 513–530, doi: 10.1007/s12594-014-0160-9.

Christensen, N.I. & Mooney, W.D. 1995. Seismic velocity structure and composition of the continental crust: A global view. *Journal of Geophysical Research*, **100**, 9761–9788, doi: 10.1029/95JB00259.

Clerc, C., Jolivet, L. & Ringenbach, J.-C. 2015. Ductile extensional shear zones in the lower crust of a passive margin. *Earth and Planetary Science Letters*, **431**, 1–7, doi: 10.1016/j.epsl.2015.08.038.

Coffin, M.F., Pringle, M.S., Duncan, R.A., Gladczenko, T.P., Storey, M., Müller, R.D. & Gahagan, L.A. 2002. Kerguelen Hotspot Magma Output since 130 Ma. *Journal of Petrology*, **43**, 1121–1137, doi: 10.1093/petrology/43.7.1121.

Curray, J.R. & Munasinghe, T. 1991. Origin of the Rajmahal Traps and the 85°E Ridge: Preliminary reconstructions of the trace of the Crozet hotspot. *Geology*, **19**, 1237, doi: 10.1130/0091-7613(1991)019<1237:OOTRTA>2.3.CO;2.

Davis, J.K. & Lavier, L.L. 2017. Influences on the development of volcanic and magma-poor morphologies during passive continental rifting. *Geosphere*, **13**, 1524–1540, doi: 10.1130/GES01538.1.

Desmurs, L., Manatschal, G. & Bernoulli, D. 2001. The Steinmann Trinity revisited: mantle exhumation and magmatism along an ocean-continent transition: the Platta nappe, eastern Switzerland. *In*: Wilson, R. C. L., Whitmarsh, R. B., Taylor, B. & Froitzheim, N. (eds) Non-Volcanic Rifting of Continental Margins. *Geological Society, London, Special Publications*, **187**, 235–266, doi: 10.1144/GSL.SP.2001.187.01.12.

Desmurs, L., Müntener, O. & Manatschal, G. 2002. Onset of magmatic accretion within a magma-poor rifted margin: a case study from the Platta ocean-continent transition, eastern Switzerland. *Contributions to Mineralogy and Petrology*, **144**, 365–382, doi: 10.1007/s00410-002-0403-4.

Dick, H.J.B., Lin, J. & Schouten, H. 2003. An ultraslow-spreading class of ocean ridge. *Nature*, **426**, 405–412, doi: 10.1038/nature02128.

Doré, T. & Lundin, E. 2015. Hyperextended continental margins — Knowns and unknowns. **43**, 95–96, doi: 10.1016/0040.

Duncan, R.A., Larsen, H.C. & Allan, J.F. (eds). 1996. *Proceedings of the Ocean Drilling Program, 163 Initial Reports*. Ocean Drilling Program, Proceedings of the Ocean Drilling Program, doi: 10.2973/odp.proc.ir.163.1996.

Eagles, G., Perez-Diaz, L. & Scarselli, N. 2015. Getting over Continent Ocean boundaries. *Earth Science Reviews*, 1–56, doi: 10.1016/j.earscirev.2015.10.009.

Eldholm, O., Thiede, J. & Taylor, E. (eds). 1987. *Proceedings of the Ocean Drilling Program, 104 Initial Reports*. Ocean Drilling Program, Proceedings of the Ocean Drilling Program, doi: 10.2973/odp.proc.ir.104.1987.

Eldholm, O., Thiede, J. & Taylor, E. 1989. Evolution of the Vøring Volcanic Margin. *In*: *Proceedings of the Ocean Drilling Program, 104 Scientific Results*. Ocean Drilling Program., doi: 10.2973/odp.proc.sr.104.191.1989.

Fletcher, R., Kusznir, N. & Cheadle, M. 2009. Melt initiation and mantle exhumation at the Iberian rifted margin: Comparison of pure–shear and upwelling-divergent flow models of continental breakup. *Comptes Rendus Geoscience*, **341**, 394–405, doi: 10.1016/j.crte.2008.12.008.

Franke, D. 2013. Rifting, lithosphere breakup and volcanism: Comparison of magma-poor and volcanic rifted margins. *Marine and Petroleum Geology*, **43**, 63–87, doi: 10.1016/j.marpetgeo.2012.11.003.

Franke, D., Neben, S., Ladage, S., Schreckenberger, B. & Hinz, K. 2007. Margin segmentation and volcano-tectonic architecture along the volcanic margin off Argentina/Uruguay, South Atlantic. *Marine Geology*, **244**, 46–67, doi: 10.1016/j.margeo.2007.06.009.

Franke, D., Ladage, S., et al. 2010. Birth of a volcanic margin off Argentina, South Atlantic. *Geochemistry, Geophysics, Geosystems*, **11**, doi: 10.1029/2009GC002715.

Frizon De Lamotte, D., Fourdan, B., Leleu, S., Leparmentier, F. & Clarens, P. 2015. Style of rifting and the stages of Pangea breakup. *Tectonics*, 1–21, doi: 10.1002/2014TC003760.Received.

Gaina, C., Müller, R.D., Brown, B.J. & Ishihara, T. 2003. Microcontinent formation around Australia. *In*: *Special Paper 372: Evolution and Dynamics of the Australian Plate*. Geological Society of America, 405–416., doi: 10.1130/0-8137-2372-8.405.

Gaina, C., Müller, R.D., Brown, B., Ishihara, T. & Ivanov, S. 2007. Breakup and early seafloor spreading between India and Antarctica. *Geophysical Journal International*, **170**, 151–169, doi: 10.1111/j.1365-246X.2007.03450.x.

Geoffroy, L. 2005. Volcanic passive margins. *Comptes Rendus Geoscience*, **337**, 1395–1408, doi: 10.1016/j.crte.2005.10.006.

Geoffroy, L., Le Gall, B., Daoud, M.A. & Jalludin, M. 2014. Flip-flop detachment tectonics at nascent passive margins in SE Afar. *Journal of the Geological Society*, **171**, 689–694, doi: 10.1144/jgs2013-135.

Geoffroy, L., Burov, E.B. & Werner, P. 2015. Volcanic passive margins: another way to break up continents. *Scientific Reports*, **5**, 14828, doi: 10.1038/srep14828.

Gernigon, L., Blischke, A., Nasuti, A. & Sand, M. 2015. Conjugate volcanic rifted margins, seafloor spreading, and microcontinent: Insights from new high-resolution aeromagnetic surveys in the Norway Basin. *Tectonics*, n/a-n/a, doi: 10.1002/2014TC003717.

Gibson, S.A., Thompson, R.N. & Day, J.A. 2006. Timescales and mechanisms of plume–lithosphere interactions: 40Ar/39Ar geochronology and geochemistry of alkaline igneous rocks from the Paraná–Etendeka large igneous province. *Earth and Planetary Science Letters*, **251**, 1–17, doi: 10.1016/j.epsl.2006.08.004.

Gillard, M., Autin, J., Manatschal, G., Sauter, D., Munschy, M. & Schaming, M. 2015. Tectonomagmatic evolution of the final stages of rifting along the deep conjugate Australian-Antarctic magma-poor rifted margins: Constraints from seismic observations. *Tectonics*, **34**, 753–783, doi: 10.1002/2015TC003850.

Gillard, M., Autin, J. & Manatschal, G. 2016a. Fault systems at hyper-extended rifted margins and embryonic oceanic crust: Structural style, evolution and relation to magma. *Marine and Petroleum Geology*, **76**, 51–67, doi: 10.1016/j.marpetgeo.2016.05.013.

Gillard, M., Manatschal, G. & Autin, J. 2016b. How can asymmetric detachment faults generate symmetric Ocean Continent Transitions? *Terra Nova*, **28**, 27–34, doi: 10.1111/ter.12183.

Gillard, M., Sauter, D., Tugend, J., Tomasi, S., Epin, M.-E. & Manatschal, G. 2017. Birth of an oceanic spreading center at a magma-poor rift system. *Scientific Reports*, **7**, 15072, doi: 10.1038/s41598-017-15522-2.

Gladczenko, T.P., Hinz, K., Eldhom, O., Meyer, H., Neben, S. & Skogseid, J. 1997. South Atlantic volcanic margins. *Journal of the Geological Society*, **154**, 465–470, doi:

10.1144/gsjgs.154.3.0465.

Gladczenko, T.P., Skogseid, J. & Eldhom, O. 1998. Namibia volcanic margin. *Marine Geophysical Researches*, **20**, 313–341, doi: 10.1023/A:1004746101320.

Haupert, I., Manatschal, G., Decarlis, A. & Unternehr, P. 2016. Upper-plate magma-poor rifted margins: Stratigraphic architecture and structural evolution. *Marine and Petroleum Geology*, **69**, 241–261, doi: 10.1016/j.marpetgeo.2015.10.020.

Heine, C., Zoethout, J. & Müller, R.D. 2013. Kinematics of the South Atlantic rift. *Solid Earth*, **4**, 215–253, doi: 10.5194/se-4-215-2013.

Hinz, K. 1981. A hypothesis on terrestrial catastrophes: Wedges of very thick oceanward dipping layers beneath passive margins; their origin and paleoenvironment significance. *Geologiches Jahrbuch*, 345–363.

Hopper, J.R., Dahl-Jensen, T., et al. 2003. Structure of the SE Greenland margin from seismic reflection and refraction data: Implications for nascent spreading center subsidence and asymmetric crustal accretion during North Atlantic opening. *Journal of Geophysical Research: Solid Earth*, **108**, 61–64, doi: 10.1029/2002JB001996.

Hopper, J.R., Funck, T., et al. 2004. Continental breakup and the onset of ultraslow seafloor spreading off Flemish Cap on the Newfoundland rifted margin. *Geology*, **32**, 93, doi: 10.1130/G19694.1.

Jagoutz, O., Müntener, O., Manatschal, G., Rubatto, D., Péron-Pinvidic, G., Turrin, B.D. & Villa, I.M. 2007. The rift-to-drift transition in the North Atlantic: A stuttering start of the MORB machine? *Geology*, **35**, 1087, doi: 10.1130/G23613A.1.

Kent, R.W., Pringle, M.S., Müller, R.D., Saunders, A.D. & Ghose, N.C. 2002. 40Ar/39Ar geochronology of the Rajmahal basalts, India, and their relationship to the Kerguelen Plateau. *Journal of Petrology*, **43**, 1141–1153, doi: 10.1093/petrology/43.7.1141.

Koopmann, H., Franke, D., Schreckenberger, B., Schulz, H., Hartwig, A. & Stollhofen, H. 2014. Segmentation and volcano-tectonic characteristics along the SW African continental margin , South Atlantic , as derived from multichannel seismic and potential fi eld data. *Marine and Petroleum Geology*, **50**, 22–39, doi: 10.1016/j.marpetgeo.2013.10.016.

Lal, N.K., Siawal, A. & Kaul, A. K. 2009. Evolution of east coast of India—A plate tectonic reconstruction. *Journal of the Geological Society of India*, **73**, 249–260.

Larsen, H.C. & Saunders, A.D. 1998. Tectonism and volcanism at the southeast Greenland rifted margin: a record of plume impact and later continental rupture. *In*: *Proceedings of the Ocean Drilling Program, 152 Scientific Results*. Ocean Drilling Program., doi: 10.2973/odp.proc.sr.152.240.1998.

Larsen, H.C., Saunders, A.D. & Clift, P.D. (eds). 1994. *Proceedings of the Ocean Drilling Program, 152 Initial Reports*. Ocean Drilling Program, Proceedings of the Ocean Drilling Program, doi: 10.2973/odp.proc.ir.152.1994.

Larsen, H.C., Dahl-Jensen, T. & Hopper, J.R. 1998. Crustal structure along the Leg 152 drilling transect. *In*: *Proceedings of the Ocean Drilling Program, 152 Scientific Results*. Ocean Drilling Program, 463–475., doi: 10.2973/odp.proc.sr.152.245.1998.

Lavier, L.L. & Manatschal, G. 2006. A mechanism to thin the continental lithosphere at magma-poor margins. *Nature*, **440**, 324–328, doi: 10.1038/nature04608.

Lundin, E.R. & Dore, A.G. 2011. Hyperextension, serpentinization, and weakening: A new paradigm for rifted margin compressional deformation. *Geology*, **39**, 347–350, doi: 10.1130/G31499.1.

Lundin, E.R., Redfield, T.F., and Peron-Pindivic, G., 2014, Rifted continental margins: Geometric influence on crustal architecture and melting. *In*: Pindell, J., Horn, B., Rosen, N.,Weimer, P., Dinkleman, M., Lowrie, A., Fillon, R., Granath, J., Kennan,

L. Sedimentary Basins: Origin, Depositional Histories, and Petroleum Systems. *33rd Annual Gulf Coast Section of the Society for Sedimentary Geology (SEPM) Foundation*, Bob F. Perkins Conference, 26–28 January, Houston, Texas, 18–53.

Manatschal, G., Sauter, D., Karpoff, A.M., Masini, E., Mohn, G. & Lagabrielle, Y. 2011. The Chenaillet Ophiolite in the French/Italian Alps: An ancient analogue for an Oceanic Core Complex? *Lithos*, **124**, 169–184, doi: 10.1016/j.lithos.2010.10.017.

Mangipudi, V.R., Goli, A., Desa, M., Tammisetti, R. & Dewangan, P. 2014. Synthesis of deep multichannel seismic and high resolution sparker data: Implications for the geological environment of the Krishna–Godavari offshore, Eastern Continental Margin of India. *Marine and Petroleum Geology*, **58**, 339–355, doi: 10.1016/j.marpetgeo.2014.08.006.

Masini, E., Manatschal, G. & Mohn, G. 2013. The Alpine Tethys rifted margins: Reconciling old and new ideas to understand the stratigraphic architecture of magma-poor rifted margins. *Sedimentology*, **60**, 174–196, doi: 10.1111/sed.12017.

Menzies, M.A., Klemperer, S.L., Ebinger, C.J. & Baker, J. 2002. Characteristics of volcanic rifted margins. *Special Paper 362: Volcanic Rifted Margins*, **362**, 1–14, doi: 10.1130/0-8137-2362-0.1.

Minshull, T. a., Dean, S.M., White, R.S. & Whitmarsh, R.B. 2001. Anomalous melt production after continental break-up in the southern Iberia Abyssal Plain. *In*: Wilson, R. C. L., Whitmarsh, R. B., Taylor, B. & Froitzheim, N. (eds) Non-Volcanic Rifting of Continental Margins. *Geological Society, London, Special Publications*, **187**, 537-550.

Mohn, G., Manatschal, G., Beltrando, M., Masini, E. & Kusznir, N. 2012. Necking of continental crust in magma-poor rifted margins: Evidence from the fossil Alpine Tethys margins. *Tectonics*, **31**, n/a-n/a, doi: 10.1029/2011TC002961.

Moulin, M., Aslanian, D. & Unternehr, P. 2010. A new starting point for the South and Equatorial Atlantic Ocean. *Earth-Science Reviews*, **98**, 1–37, doi: 10.1016/j.earscirev.2009.08.001.

Müntener, O. & Manatschal, G. 2006. High degrees of melt extraction recorded by spinel harzburgite of the Newfoundland margin: The role of inheritance and consequences for the evolution of the southern North Atlantic. *Earth and Planetary Science Letters*, **252**, 437–452, doi: 10.1016/j.epsl.2006.10.009.

Müntener, O., Pettke, T., Desmurs, L., Meier, M. & Schaltegger, U. 2004. Refertilization of mantle peridotite in embryonic ocean basins: trace element and Nd isotopic evidence and implications for crust–mantle relationships. *Earth and Planetary Science Letters*, **221**, 293–308, doi: 10.1016/S0012-821X(04)00073-1.

Muntener, O. & Piccardo, G.B. 2003. Melt migration in ophiolitic peridotites: the message from Alpine-Apennine peridotites and implications for embryonic ocean basins. *In*: Dilek, Y. & Robinson, P. T., (eds) Ophiolites in Earth History. *Geological Society, London, Special Publications*, **218**, 69–89, doi: 10.1144/GSL.SP.2003.218.01.05.

Muntener, O., Manatschal, G., Desmurs, L. & Pettke, T. 2010. Plagioclase Peridotites in Ocean-Continent Transitions: Refertilized Mantle Domains Generated by Melt Stagnation in the Shallow Mantle Lithosphere. *Journal of Petrology*, **51**, 255–294, doi: 10.1093/petrology/egp087.

Mutter, J.C. 1985. Seaward dipping reflectors and the continent-ocean boundary at passive continental margins. *Tectonophysics*, **114**, 117–131, doi: 10.1016/0040-1951(85)90009-5.

Mutter, J.C. 1993. Margins declassified. *Nature*, **364**, 393–394, doi: 10.1038/364393a0.

Mutter, J.C., Talwani, M. & Stoffa, P.L. 1982. Origin of seaward-dipping reflectors in oceanic crust off the Norwegian margin by ‘subaerial sea-floor spreading’. *Geology*, **10**, 353, doi: 10.1130/0091-7613(1982)10<353:OOSRIO>2.0.CO;2.

Mutter, J.C., Buck, W.R. & Zehnder, C.M. 1988. Convective partial melting: 1. A model for the formation of thick basaltic sequences during the initiation of spreading. *Journal of Geophysical Research*, **93**, 1031, doi: 10.1029/JB093iB02p01031.

Nemčok, M., Sinha, S.T., et al. 2013. East Indian margin evolution and crustal architecture: integration of deep reflection seismic interpretation and gravity modelling. *In:* Mohriak, W. U., Danforth, A., Post, P. J., Brown, D. E., Tari, G. C., Nemčok, M., & Sinha, S. T. (eds) Conjugate Divergent Margins. *Geological Society, London, Special Publications*, **369**, 477–496, doi: 10.1144/SP369.6.

Nielsen, T.K. & Hopper, J.R. 2004. From rift to drift: Mantle melting during continental breakup. *Geochemistry, Geophysics, Geosystems*, **5**, doi: 10.1029/2003GC000662.

Nirrengarten, M., Gernigon, L. & Manatschal, G. 2014. Nature, structure and age of Lower Crustal Bodies in the Møre volcanic rifted margin: facts and uncertainties. *Tectonophysics*, 59, doi: 10.1016/j.tecto.2014.08.004.

Olierook, H.K.H., Jourdan, F., Merle, R.E., Timms, N.E., Kusznir, N. & Muhling, J.R. 2016. Bunbury Basalt: Gondwana breakup products or earliest vestiges of the Kerguelen mantle plume? *Earth and Planetary Science Letters*, **440**, 20–32, doi: 10.1016/j.epsl.2016.02.008.

Paton, D.A., Pindell, J., McDermott, K., Bellingham, P. & Horn, B. 2017. Evolution of seaward-dipping reflectors at the onset of oceanic crust formation at volcanic passive margins: Insights from the South Atlantic. *Geology*, **45**, 439–442, doi: 10.1130/G38706.1.

Peate, D.W. 1997. The Paraná–Etendeka Province. *In*: Mahoney, J.J., Coffin, M.F. Large Igneous Provinces: Continental, Oceanic, and Planetary Flood Volcanism, *American Geophysical Union*, **100**, 217-245.

Pérez-Gussinyé, M. & Reston, T.J. 2001. Rheological evolution during extension at nonvolcanic rifted margins: Onset of serpentinization and development of detachments leading to continental breakup. *Journal of Geophysical Research: Solid Earth*, **106**, 3961–3975, doi: 10.1029/2000JB900325.

Pérez-Gussinyé, M., Morgan, J.P., Reston, T.J. & Ranero, C.R. 2006. The rift to drift transition at non-volcanic margins: Insights from numerical modelling. *Earth and Planetary Science Letters*, **244**, 458–473, doi: 10.1016/j.epsl.2006.01.059.

Peron-pinvidic, G., Osmundsen, P.T. & Ebbing, J. 2016. Mismatch of geophysical datasets in distal rifted margin studies. *Terra Nova*, **28**, 340–347, doi: 10.1111/ter.12226.

Peron-Pinvidic, G. & Osmundsen, P.T. 2016. Architecture of the distal and outer domains of the Mid-Norwegian rifted margin: Insights from the Rån-Gjallar ridges system. *Marine and Petroleum Geology*, **77**, 280–299, doi: 10.1016/j.marpetgeo.2016.06.014.

Peron-Pinvidic, G., Shillington, D.J. & Tucholke, B.E. 2010. Characterization of sills associated with the U reflection on the Newfoundland margin: Evidence for widespread early post-rift magmatism on a magma-poor rifted margin. *Geophysical Journal International*, **182**, 113–136, doi: 10.1111/j.1365-246X.2010.04635.x.

Peron-Pinvidic, G., Manatschal, G. & Osmundsen, P.T. 2013. Structural comparison of archetypal Atlantic rifted margins: A review of observations and concepts. *Marine and Petroleum Geology*, **43**, 21–47, doi: 10.1016/j.marpetgeo.2013.02.002.

Péron-Pinvidic, G. & Manatschal, G. 2009. The final rifting evolution at deep magma-poor passive margins from Iberia-Newfoundland: A new point of view. *International Journal of Earth Sciences*, **98**, 1581–1597, doi: 10.1007/s00531-008-0337-9.

Peron-Pinvidic, G., Manatschal, G., Masini, E., Sutra, E., Flament, J.M., Haupert, I. & Unternehr, P. 2017. Unravelling the along-strike variability of the Angola-Gabon rifted margin: a mapping approach. *In*: Sabato Ceraldi, T., Hodgkinson, R. A., Backe, G. Petroleum Geoscience of the West Africa Margin. *Geological Society, London, Special Publications*, 438, doi: 10.1144/SP438.1.

Picazo, S., Müntener, O., Manatschal, G., Bauville, A., Karner, G. & Johnson, C. 2016. Mapping the nature of mantle domains in Western and Central Europe based on clinopyroxene and spinel chemistry: Evidence for mantle modification during an extensional cycle. *Lithos*, **266**–**267**, 233–263, doi: 10.1016/j.lithos.2016.08.029.

Pindell, J., Graham, R. & Horn, B. 2014. Rapid outer marginal collapse at the rift to drift transition of passive margin evolution, with a Gulf of Mexico case study. *Basin Research*, **26**, 701–725, doi: 10.1111/bre.12059.

Planke, S., Symonds, P.A., Alvestad, E. & Skogseid, J. 2000. Seismic volcanostratigraphy of large-volume basaltic extrusive complexes on rifted margins. *Journal of Geophysical Research*, **105**, 19335–19351, doi: 10.1029/1999JB900005.

Planke, S., Rasmussen, T., Rey, S.S. & Myklebust, R. 2005. Seismic characteristics and distribution of volcanic intrusions and hydrothermal vent complexes in the Vøring and Møre basins. *Petroleum Geology: North-West Europe and Global Perspectives*, 833–844, doi: 10.1144/0060833.

Powell, C.M., Roots, S.R. & Veevers, J.J. 1988. Pre-breakup continental extension in East Gondwanaland and the early opening of the eastern Indian Ocean. *Tectonophysics*, **155**, 261–283, doi: 10.1016/0040-1951(88)90269-7.

Rabinowitz, P.D. & LaBrecque, J. 1979. The Mesozoic South Atlantic Ocean and evolution of its continental margins. *Journal of Geophysical Research*, **84**, 5973, doi: 10.1029/JB084iB11p05973.

Radhakrishna, M., Subrahmanyam, C. & Damodharan, T. 2010. Thin oceanic crust below Bay of Bengal inferred from 3-D gravity interpretation. *Tectonophysics*, **493**, 93–105, doi: 10.1016/j.tecto.2010.07.004.

Radhakrishna, M., Twinkle, D., Nayak, S., Bastia, R. & Rao, G.S. 2012. Crustal structure and rift architecture across the Krishna-Godavari basin in the central Eastern Continental Margin of India based on analysis of gravity and seismic data. *Marine and Petroleum Geology*, **37**, 129–146, doi: 10.1016/j.marpetgeo.2012.05.005.

Ramana, M.V., Nair, R.R., et al. 1994. Mesozoic anomalies in the Bay of Bengal. *Earth and Planetary Science Letters*, **121**, 469–475, doi: 10.1016/0012-821X(94)90084-1.

Reeves, C. & de Wit, M. 2000. Making ends meet in Gondwana: retracing the transforms of the Indian Ocean and reconnecting continental shear zones. *Terra Nova*, **12**, 272–280, doi: 10.1046/j.1365-3121.2000.00309.x.

Reston, T. & Manatschal, G. 2011. Rifted Margins: Building Blocks of Later Collision. 3–21., doi: 10.1007/978-3-540-88558-0_1.

Reston, T.J. 2009. The structure, evolution and symmetry of the magma-poor rifted margins of the North and Central Atlantic: A synthesis. *Tectonophysics*, **468**, 6–27, doi: 10.1016/j.tecto.2008.09.002.

Roberts, D.G. & Schnitker, D. 1984. *Initial Reports of the Deep Sea Drilling Project, 81*. U.S. Government Printing Office, Initial Reports of the Deep Sea Drilling Project, doi: 10.2973/dsdp.proc.81.1984.

Rooney, T.O., Nelson, W.R., Ayalew, D., Hanan, B., Yirgu, G. & Kappelman, J. 2017. Melting the lithosphere : Metasomes as a source for mantle-derived magmas. *Earth and Planetary Science Letters*, **461**, 105–118, doi: 10.1016/j.epsl.2016.12.010.

Rooney, T.O., Nelson, W.R., Dosso, L., Furman, T. & Hanan, B. 2014. The role of continental lithosphere metasomes in the production of HIMU-like magmatism on the northeast African and Arabian plates. *Geology*, **42**, 419–422, doi: 10.1130/G35216.1.

Sandwell, D.T., Müller, R.D., Smith, W.H.F., Garcia, E. & Francis, R. 2014. New global marine gravity model from CryoSat-2 and Jason-1 reveals buried tectonic structure. *Science (New York, N.Y.)*, **346**, 65–67, doi: 10.1126/science.1258213.

Saunders, A.D., Larsen, H.C. & Fitton, J.G. 1998. Magmatic development of the southeast Greenland Margin and evolution of the Iceland Plume: geochemical constraints from Leg 152. *In*: *Proceedings of the Ocean Drilling Program, 152 Scientific Results*. Ocean Drilling Program, 479–501., doi: 10.2973/odp.proc.sr.152.239.1998.

Sauter, D., Unternehr, P., et al. 2016. Evidence for magma entrapment below oceanic crust from deep seismic reflections in the Western Somali Basin. *Geology*, **44**, G37747.1, doi: 10.1130/G37747.1.

Sawyer, D.S., Coffin, M.F., Reston, T.J., Stock, J.M. & Hopper, J.R. 2007. COBBOOM: The Continental Breakup and Birth of Oceans Mission. *Scientific Drilling*, 13–25, doi: 10.2204/iodp.sd.5.02.2007.

Shipboard Scientific Party. 1998. Site 1070. *In:* Whitmarsh, R. B., Beslier, M.-O. et al, *Proceedings of the ODP, Initial Reports,* **173**, Ocean Drilling Program, College Station, TX, 265–294. doi:10.2973/odp.proc.ir.173.108.1998

Shipboard Scientific Party. 2004. Site 1277. *In:* Tucholke, B.E., Sibuet, J.-C., Klaus, A., et al., *Proceedings of the ODP, Initial Reports,* **210**, Ocean Drilling Program, College Station, TX, 1–39. doi:10.2973/odp.proc.ir.210.104.2004

Sibuet, J. & Tucholke, B.E. 2013. The geodynamic province of transitional lithosphere adjacent to magma-poor continental margins. *In:* Mohriak, W. U., Danforth, A., Post, P. J., Brown, D. E., Tari, G. C., Nemčok, M., & Sinha, S. T. (eds) Conjugate Divergent Margins. *Geological Society, London, Special Publications*, **369**, 429–452, doi: 10.1144/SP369.15.

Sinha, S.T., Nemčok, M., Choudhuri, M., Sinha, N. & Rao, D.P. 2016. The role of break-up localization in microcontinent separation along a strike-slip margin: the East India-Elan Bank case study. *In*: Nemčok, M., Rybár, S., Sinha, S. T., Hermeston, S. A., Ledvényiová, L. (eds) Transform Margins: Development, Controls and Petroleum Systems. *Geological Society, London, Special Publications*, doi: 10.1144/SP431.5.

Skogseid, J. 2001. Volcanic margins: geodynamic and exploration aspects. *Marine and Petroleum Geology*, **18**, 457–461, doi: 10.1016/S0264-8172(00)00070-2.

Skogseid, J., Planke, S., Faleide, J.I., Pedersen, T., Eldholm, O. & Neverdal, F. 2000. NE Atlantic continental rifting and volcanic margin formation. *In*: Nøttvedt, A. Dynamics of the Norwegian Margin. *Geological Society, London, Special Publications*, **167**, 295–326, doi: 10.1144/GSL.SP.2000.167.01.12

Soto, M., Morales, E., Veroslavsky, G., de Santa Ana, H., Ucha, N. & Rodríguez, P. 2011. The continental margin of Uruguay: Crustal architecture and segmentation. *Marine and Petroleum Geology*, **28**, 1676–1689, doi: 10.1016/j.marpetgeo.2011.07.001.

Stab, M., Bellahsen, N., Pik, R., Quidelleur, X., Ayalew, D. & Leroy, S. 2016. Modes of rifting in magma-rich settings: Tectono-magmatic evolution of Central Afar. *Tectonics*, 2–38, doi: 10.1002/2015TC003893.

Stewart, K., Turner, S., Kelley, S., Hawkesworth, C., Kirstein, L. & Mantovani, M. 1996. 3-D, 40Ar/39Ar geochronology in the Paraná continental flood basalt province. *Earth and Planetary Science Letters*, **143**, 95–109, doi: 10.1016/0012-821X(96)00132-X.

Stica, J.M., Zalán, P.V. & Ferrari, A.L. 2014. The evolution of rifting on the volcanic margin of the Pelotas Basin and the contextualization of the Paraná–Etendeka LIP in the separation of Gondwana in the South Atlantic. *Marine and Petroleum Geology*, **50**, 1–21, doi: 10.1016/j.marpetgeo.2013.10.015.

Stoakes, F.A., Campbell, C.V., Cass, R. & Ucha, N. 1991. Seismic Stratigraphic Analysis of the Punta Del Este Basin, Offshore Uruguay, South America. *AAPG Bulletin*, **75**, 219–240.

Subrahmanyam, C. & Chand, S. 2006. Evolution of the passive continental margins of India-a geophysical appraisal. *Gondwana Research*, **10**, 167–178, doi: 10.1016/j.gr.2005.11.024.

Sutra, E., Manatschal, G., Mohn, G. & Unternehr, P. 2013. Quantification and restoration of extensional deformation along the Western Iberia and Newfoundland rifted margins. *Geochemistry, Geophysics, Geosystems*, **14**, 2575–2597, doi: 10.1002/ggge.20135.

Talwani, M., Desa, M.A., Ismaiel, M. & Sree Krishna, K. 2016. The Tectonic origin of the Bay of Bengal and Bangladesh. *Journal of Geophysical Research: Solid Earth*, **121**, 4836–4851, doi: 10.1002/2015JB012734.

Torsvik, T.H., Rousse, S., Labails, C. & Smethurst, M.A. 2009. A new scheme for the opening of the South Atlantic Ocean and the dissection of an Aptian salt basin. *Geophysical Journal International*, **177**, 1315–1333, doi: 10.1111/j.1365-246X.2009.04137.x.

Tugend, J., Manatschal, G., Kusznir, N.J. & Masini, E. 2015. Characterizing and identifying structural domains at rifted continental margins: application to the Bay of Biscay margins and its Western Pyrenean fossil remnants. *In*: Gibson, G. M., Roure,F.&Manatschal, G. (eds) Sedimentary Basins and Crustal Processes at Continental Margins: From Modern Hyper-extended Margins to Deformed Ancient Analogues. *Geological Society, London, Special Publications*, **413**, 171–203, doi: 10.1144/SP413.3.

Turner, S., Regelous, M., Kelley, S., Hawkesworth, C. & Mantovani, M. 1994. Magmatism and continental break-up in the South Atlantic: high precision40Ar-39Ar geochronology. *Earth and Planetary Science Letters*, **121**, 333–348, doi: 10.1016/0012-821X(94)90076-0.

Welford, J.K., Smith, J.A., Hall, J., Deemer, S., Srivastava, S.P. & Sibuet, J.-C. 2010. Structure and rifting evolution of the northern Newfoundland Basin from Erable multichannel seismic reflection profiles across the southeastern margin of Flemish Cap. *Geophysical Journal International*, **180**, 976–998, doi: 10.1111/j.1365-246X.2009.04477.x.

White, R. & McKenzie, D. 1989. Magmatism at rift zones: The generation of volcanic continental margins and flood basalts. *Journal of Geophysical Research*, **94**, 7685, doi: 10.1029/JB094iB06p07685.

White, r. S., mckenzie, d. & o'nions, r. K. 1992. Oceanic crustal thickness from seismic measurements and rare earth element inversions, *Journal of Geophysical Research*, ***97***, 19683, doi:10.1029/92JB01749.

White, R.S., Smith, L.K., Roberts, A.W., Christie, P.A.F. & Kusznir, N.J. 2008. Lower-crustal intrusion on the North Atlantic continental margin. **452**, 460–465, doi: 10.1038/nature06687.

Whitmarsh, R.B., Manatschal, G. & Minshull, T.A. 2001a. Evolution of magma-poor continental margins from rifting to seafloor spreading. *Nature*, **413**, 150–154, doi: 10.1038/35093085.

Whitmarsh, R.B., Minshull, T.A., Russell, S.M., Dean, S.M., Louden, K.E. & Chian, D. 2001b. The role of syn-rift magmatism in the rift-to-drift evolution of the West Iberia continental margin: geophysical observations. *In*: Wilson, R. C. L., Whitmarsh, R. B., Taylor, B. & Froitzheim, N. (eds) Non-Volcanic Rifting of Continental Margins. *Geological Society, London, Special Publications*, **187**, 107–124, doi: 10.1144/GSL.SP.2001.187.01.06.

Wilson, R.C.L., Manatschal, G. & Wise, S. 2001. Rifting along non-volcanic passive margins: stratigraphic and seismic evidence from the Mesozoic successions of the Alps and western Iberia. *In*: WILSON, R. C. L., WHITMARSH, R. B., TAYLOR, B. & FROITZHEIM, N. (eds) Non-Volcanic Rifting of Continental Margins. *Geological Society, London, Special Publications*, **187**, 429–452., doi: 10.1144/GSL.SP.2001.187.01.21.

FIGURE CAPTIONS:

Fig. 1. (**a**) Topographic/Bathymetric map of the East Indian rifted margin and Bay of Bengal (ETOPO1, Amante & Eakins 2009). (**b**) Free-air gravity anomaly map (Sandwell *et al.* 2014) showing the first-order morpho-tectonic features of the study area and location of the ION Geophysical IndiaSPAN (http://www.iongeo.com/Data_Library/India/, Nemčok *et al.* 2013; Radhakrishna *et al.* 2012). Topographic/Bathymetric contours are given every 1000m. Equidistant cylindrical projection, geographic coordinate system WGS 84.

Fig. 2. (**a**) Topographic/Bathymetric map of the South Atlantic rifted margins (ETOPO1, Amante & Eakins 2009). (**b**) Free-air gravity anomaly map of the Uruguayan segment (Sandwell *et al.* 2014). Approximate location of the UruguaySPAN as given on ION Geophysical website (http://www.iongeo.com/Data_Library/South_America/Uruguay/). First-order structures and magmatism compiled from (Gladczenko *et al.* 1997, 1998; Franke *et al.* 2007; Stica *et al.* 2014; Clerc *et al.* 2015; Koopmann *et al.* 2014). Topographic/Bathymetric contours are given every 1000m. Equidistant cylindrical projection, geographic coordinate system WGS 84. SJB, San Jorge Basin; VB, Valdes Basin; RB, Rawson Basin; CB, Colorado Basin; SB, Salado Basin; WB, Walvis Basin LB, Lüderitz Basin; OB, Orange Basin.

Fig. 3. Seismic observations from the SE-Indian rifted margin case example (PSTM and PSDM seismic profiles, courtesy of ION Geophysical). (**a**) Line drawing of the PSTM seismic profile and interpretation of first-order interfaces. (**b**) Interpretation of first-order interfaces and tectonic structures of the corresponding PSDM seismic profile (vertical exaggeration x2). Based on the evolution of accommodation space (between sea level and top basement) and crustal thickness (between top basement and seismic Moho) along the PSDM profile, we define structural margin domains: the proximal, thinned, exhumed mantle, proto-oceanic and oceanic domains. (**c**) Zoom over the interpreted exhumed mantle domain showing hints for magmatic additions possibly syn- and post-exhumation. (**d**) Zoom over the interpreted proto-oceanic domain showing top basement, intra-basement reflectivity and pattern of seismic Moho.

Fig. 4. Interpretations of the SE-Indian rifted margin case example, illustrating different scenarios for the nature of the proto-oceanic domain. (**a**) Scenario 1: igneous crust (**b**) Scenario 2: exhumed serpentinized mantle 'sandwiched' between extrusive and intrusive material (**c**) Scenario 3: exhumed serpentinized mantle 'sandwiched' between extrusive and intrusive material and melt entrapment at depth.

Fig. 5. Seismic observations from the Uruguayan rifted margin case example (PSTM and PSDM seismic profiles, courtesy of ION Geophysical). (**a**) Line drawing of the PSTM seismic profile and interpretation of first-order interfaces. (**b**) Interpretation of first-order interfaces and structures of the PSDM of the same seismic profile (vertical exaggeration x2). Based on the evolution of accommodation space (between sea level and top basement) and crustal thickness

(between top basement/base SDRs and seismic Moho) along the PSDM profile, we define structural margin domains: the proximal, thinned, proto-oceanic and oceanic domains. (**c**) Zoom over a possible volcanic edifice in the interpreted thinned domain. (**d**) Zoom over the interpreted proto-oceanic domain showing top basement, SDRs, base SDRs and continentward onlaps.

Fig. 6. Interpretations of the Uruguayan rifted margin case example, illustrating different scenarios for the nature of the proto-oceanic domain. **(a)** Scenario 1: igneous crust **(b)** Scenario 2: intruded continental crust 'sandwiched' between extrusives (SDRs) and underplated material **(c)** Scenario 3: intruded continental crust 'sandwiched' between extrusives (SDRs) and underplated material and melt entrapment at depth.

Fig. 7. Estimates of the magmatic budget at lithospheric breakup inferred from the different scenarios (1 to 3) proposed for the proto-oceanic domains at the SE-Indian (upper part) and Uruguayan examples (lower part). The evolution of magmatic addition thickness, representing the magmatic budget is indicated by the red line. The green and brown curves respectively represent the thickness of exhumed serpentinized mantle (SE- India) and continental crust (Uruguay). The dashed grey line represents the apparent total thickness of the proto-oceanic domain (ie. between top basement and seismic Moho). The thick dashed blue line represents the 7±1 km thick reference for oceanic crust thickness (White *et al.* 1992; Bown & White 1994) inferred from decompression melting models (White & McKenzie 1989). CC, continental crust; ExM, Exhumed serpentinized mantle; Proto-OC, Proto-oceanic crust; OC, oceanic crust.

Fig. 8. Interpretations of lithospheric breakup mechanisms for each of the scenarios (1 to 3) proposed for the proto-oceanic domains at the SE-Indian (upper part) and Uruguayan examples (lower part). The diagrams presented associated to each scenario, show the inferred evolution of melt production at lithospheric breakup and recorded within the proto-oceanic domain. We distinguish the 'instantaneous', 'gradual' and 'polyphase' lithospheric breakup, respectively associated to fast, progressive and variable melt production. CC, continental crust; ExM, Exhumed serpentinized mantle; Proto-OC, Proto-oceanic crust; OC, oceanic crust.

Figure 1

Click here to download Figure Fig1_Maps_India_vf.tif

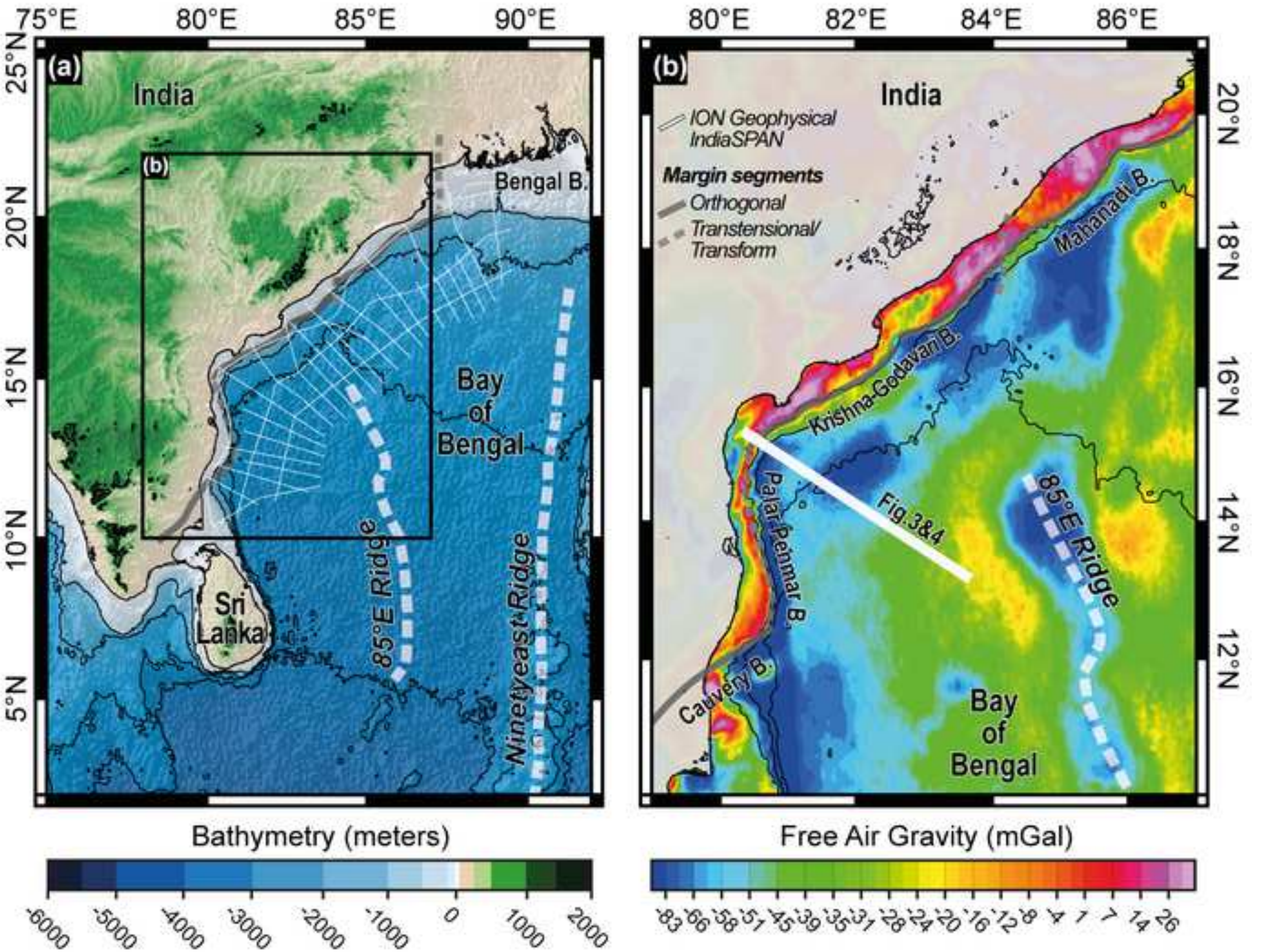

Figure 2

Click here to download Figure Fig2_Uruguay_vf.png

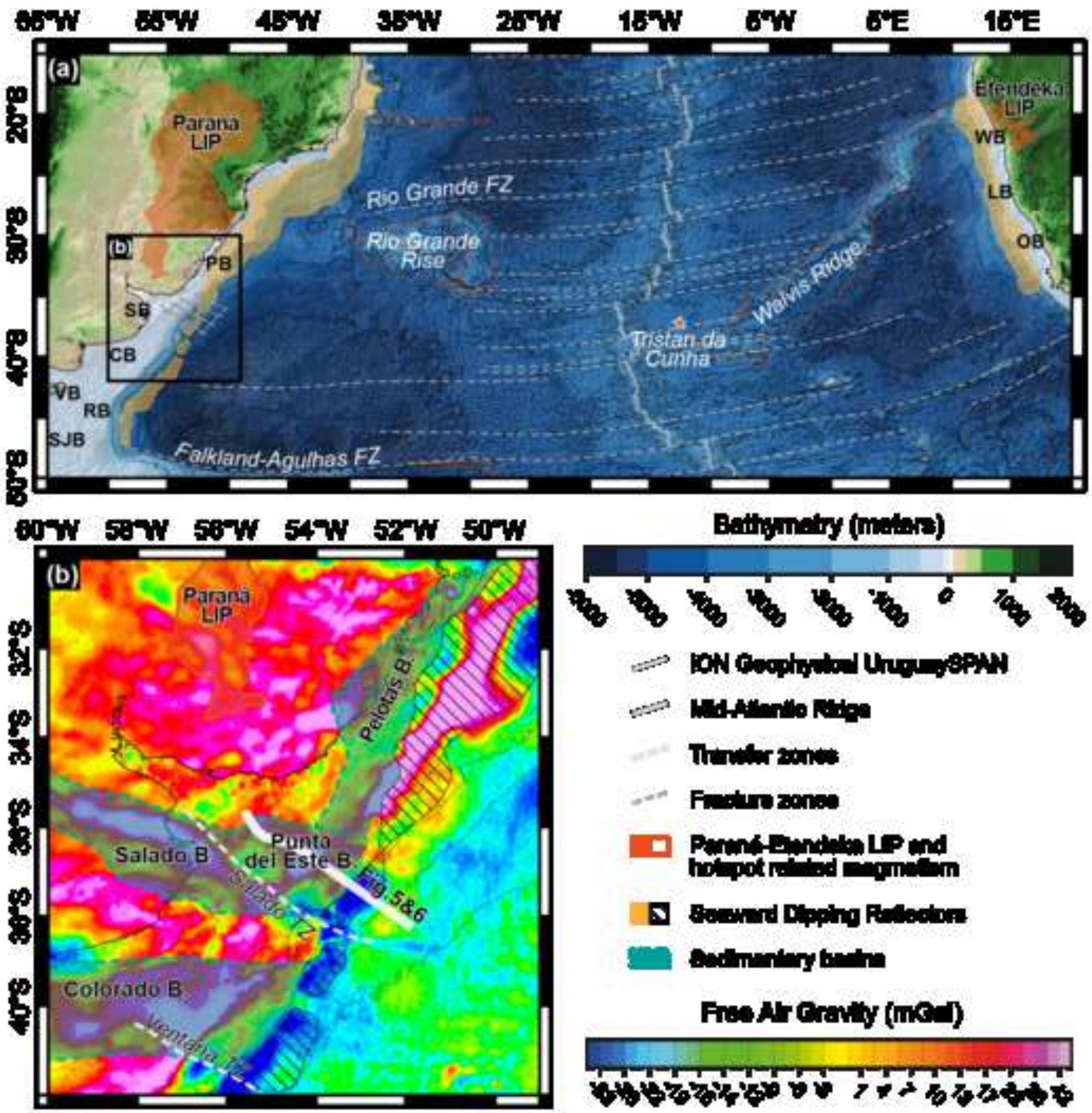

Figure 3

Click here to download Figure Fig3_LD_E-India_vf2-01.png

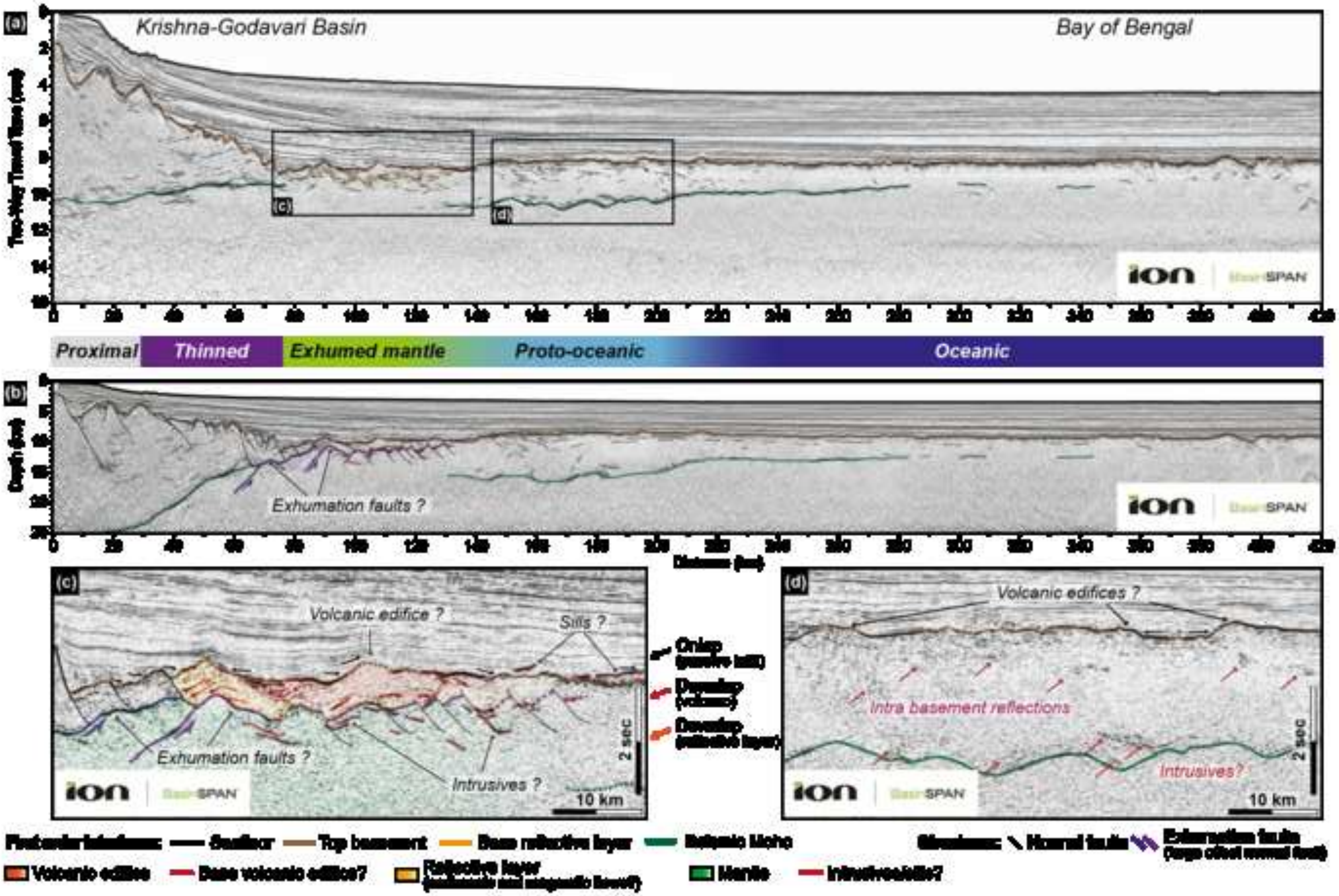

Figure 4

Click here to download Figure Fig4_Interps_India_vf.tif

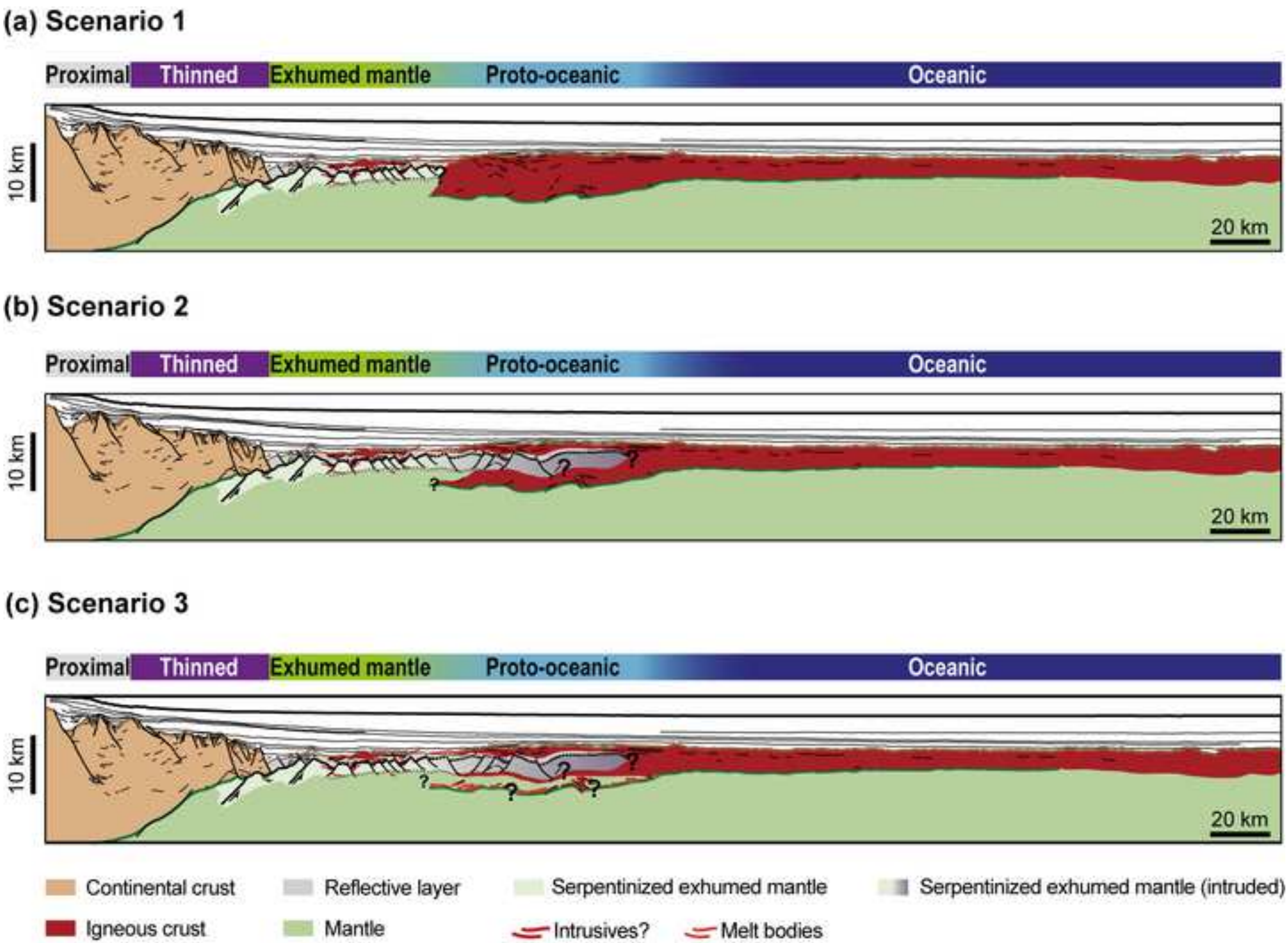

Figure 5

Click here to download Figure Fig5_LD_Uruguay_vf2-01.png

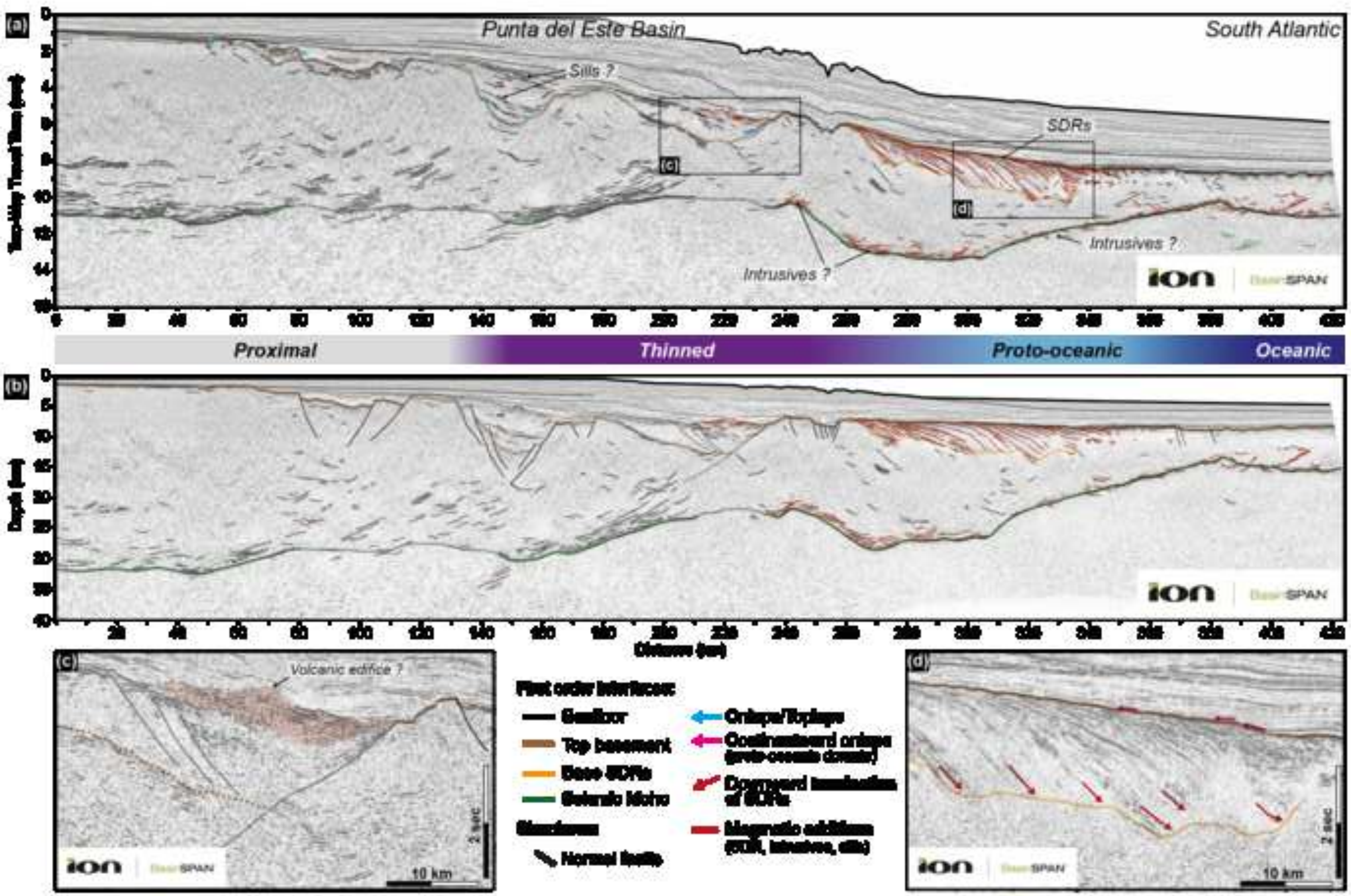

Figure 6

Click here to download Figure Fig6_Interps_Uruguay_vf.png

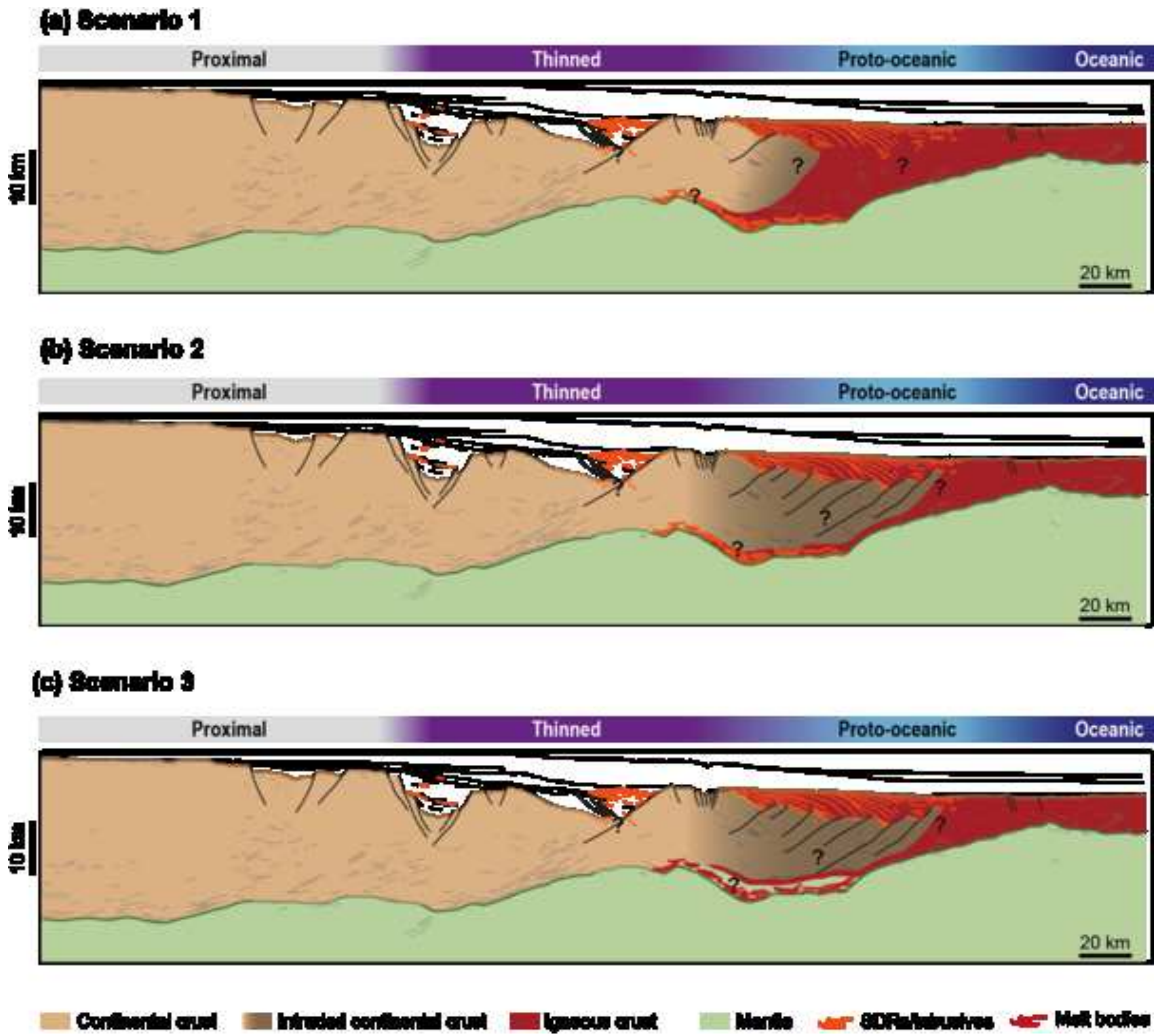

Figure 7 Click here to download Figure Fig7_OuterHigh&MagmaticBudget_vf.png

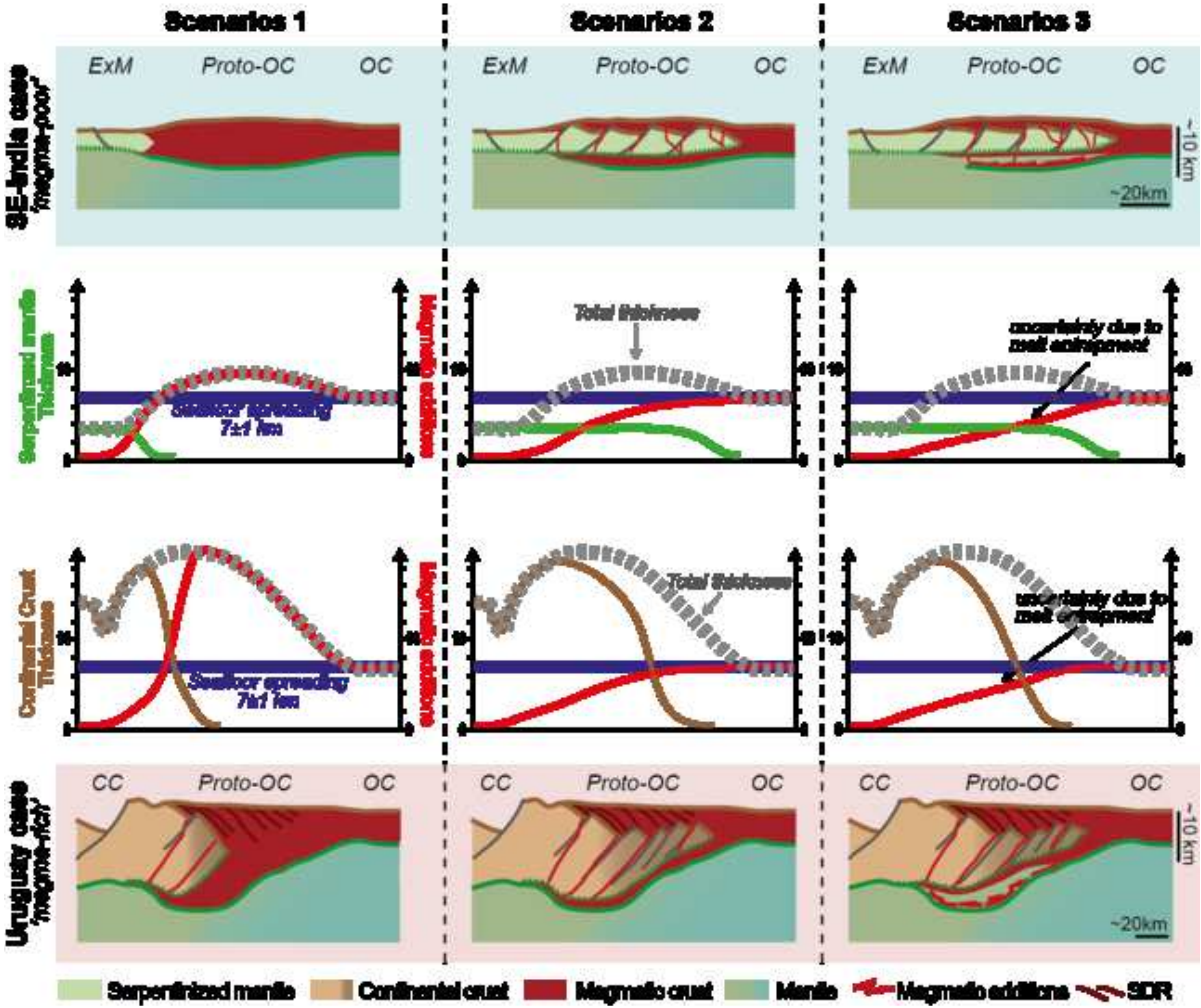

Figure 8

Click here to download Figure Fig8_BU-Process&RiftedMarginType_vf.tif